A Broadband Antenna for Ionospheric Sounding

ALEXANDER WITTE

KTH Electrical Engineering

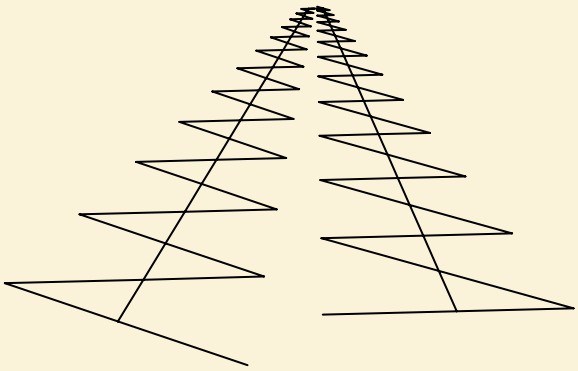

Master's Degree Project
Stockholm, Sweden June 2008

XR-EE-ETK 2008:011

KTH Electrical Engineering

A Broadband Antenna for Ionospheric Sounding

ALEXANDER WITTE

Master of Science Thesis
in Electrical Engineering
Stockholm, Sweden June 2008

Supervisor: Peter Fuks

Division of Electromagnetic Engineering,
School of Electrical Engineering
Royal Institute of Technology
SE - 100 44 Stockholm, Sweden

XR-EE-ETK 2008:011

Abstract

A broadband transmitter antenna for an ionospheric sounder at the Alfvén Laboratory in Stockholm is designed. Various broadband antenna types are examined for their broadband features as well as their geometry. A segmentation method for the simulation of broadband antennas is derived and verified. The impact of surrounding buildings and ground on antenna performance is simulated. Three different frequency independent antenna types, a log-periodic dipole array, a pyramidal log-spiral and a log-periodic zigzag antenna are modeled and simulated for frequencies from 2 to 20 MHz. A log-periodic zigzag antenna is optimized and provides reasonable input impedance over the entire bandwidth at a standing wave ratio of less then 2:1. Construction material is selected and the antenna is constructed.

Acknowledgements

I would like to express my deepest gratitude to my supervisor Peter Fuks, as well as to the initiator of this project at the Department of Space and Plasma Physics, Nickolay Ivchenko. They encouraged me throughout this study with their trust in my abilities and their enthusiasm for this project. They also provided me with the opportunity to go on a field trip, which was very rewarding. I would also like to thank Kjäll Olsson for his support and his confidence in my ideas. Furthermore, I thank Mike Rietveld at EISCAT, Norway, and Björn Gustavsson at the University of Tromsø, Norway, for their invaluable advise and inspiration during and after the NEMI campaign 2008. I am also in debt to Jean-Marc Battini at the department of Mechanics for his consultation, to Bill Wright and Richard N. Grubb for sharing their work and, last but not least, to Mohan Pakkurti for proofreading this report.

Alexander Witte
Stockholm, June 2008

Contents

Chapter 1

Introduction

> *"Nothing is too wonderful to be true if it be consistent with the laws of nature, and in such things as these, experiment is the best test of such consistency."*
>
> Michael Faraday, 19 March 1849

Indeed, it was Faraday who introduced the name *ion*[1] to describe charged atoms- and molecules. These particles occur naturally in the upper atmosphere, where the atmospheric gases are *ionized* by solar- and cosmic radiation. This region of ionized gas (or *plasma*) in the atmosphere is called *ionosphere*. One of the most fundamental instruments to investigate the ionosphere is called *ionosonde*, a radar system which detects the time delay between a transmitted radio wave and its reflection by the ionosphere.

The aim of this master's thesis was to design and to construct a transmitter antenna for such an ionosonde at the Alfvén Laboratory in Stockholm, Sweden. The report covers a detailed review of the design process including a brief antenna-type survey, as well as a description of the final construction. Prior to that, a short introduction to the ionosphere and project specifications are given hereafter.

1.1 Ionosphere

The ionosphere is a considerably recent discovery. Although one of its most remarkable effects – the aurora[2] – has fascinated humans since ancient times, little was known about the earth's upper atmosphere. It's existence had been suggested by Stewart (1878) and also earlier by Faraday (1832), Gauss (1839) and Lord Kelvin (1860). But it was first through the work with radio waves by Marconi (1901) that the research on the ionosphere truly intensified. Upon Marconi's successful transmission of a radio signal between England and America, both Kenelly and Heaviside (1902) reasoned that the observed deviation from

[1] from the Greek word ἰόν (going)

[2] Aurora Borealis (Northern Lights), named after the Roman goddess of the dawn, Aurora, and the Greek god for the cold north wind, Βορέασ (Boreas)

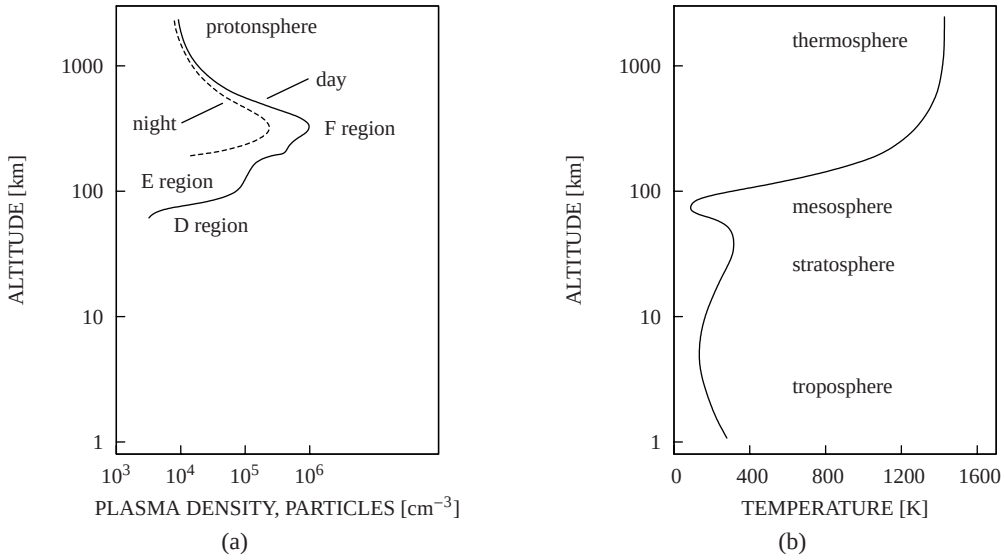

Figure 1.1: Atmospheric profiles. (a) Ionosphere, nighttime plasma density. (b) Thermal structure of the atmosphere. (After M. C. Kelley, The Earth's Ionosphere: Plasma Physics and Electrodynamics, Academic Press, 1989)

the rectilinear path can only be explained by a conducting layer at higher altitude [*Thewlis* et al., 1961, p.70]. After theories concerning the propagation of radio waves in ionized gases by Eccles (1924) and Larmor (1924), the existence of the ionosphere was finally proven through the classic experiments by Appleton and Barnett (1925) as well as by Breit and Tuve (1926) [*Whitten* and *Poppoff*, 1965, p.3]. After the Second World War, the US Navy began intense research on the ionosphere due to its role in long distance radio communication. In the meantime, the ionosphere has become a major research field for both plasma- and space physicists.

The structure of the ionosphere is very dynamic. As mentioned earlier, a major cause for ionized gases in the upper atmosphere is solar- and cosmic radiation. The physical process behind this is called photoionization. When a photon collides with a neutral atom or molecule, it ejects one or more electrons, leaving an ion and a free electron behind. Later on, ions and electrons may recombine, a reversed process that accelerates at higher electron density. Due to the dynamics between ionization and recombination as well as due to the diurnal variation of solar radiation, the structure of the ionosphere is changing constantly – especially between night and day.

However, three major *regions* of ionization can be distinguished, as visualized in figure 1.1. The *D-region* is the lowest stratum of ionization and extends up to 80km. It is mainly a daytime phenomenon and absorbs most of the lower radio frequencies. The *E-region* or *Kenelly-Heaviside* layer extends from 90 to about 120km. This layer is mainly caused by solar radiation and disappears gradually after sunset due to recombination. At times, a so

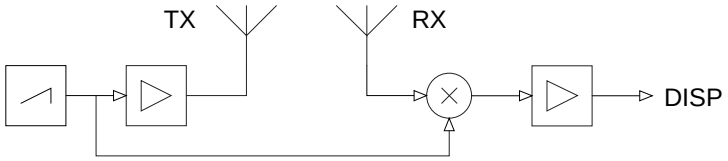

Figure 1.2: Schematics of a typical continuous-signal ionosonde

called *sporadic E-layer* or E_s*-layer* can be seen. It manifests as small clouds of intense ionization inside the E-layer, lasting from minutes up to hours and extending the range of radio wave communications exceptionally. The *F-region* or *Appleton* layer extends from about 120 to 400 km and is the only major layer present throughout the day. At night, this layer bifurcates into two layers, F_1 and F_2. Due to the temporal changes in the solar radiation as well as other dynamics like solar activity and the earth's magnetosphere, currents are forming within the ionosphere. One of the most noticeable and beautiful visual effects caused by these currents is the Aurora Borealis.

1.2 Ionosonde

An *ionosonde* is a radar system used to determine the altitude of ionospheric layers. It uses a short radio pulse directed towards the ionosphere and measures the time delay between the outbound pulse and its reflected echo. This technique was developed by Breit and Tuve for their first ionospheric experiments in 1925[3]. Meanwhile, an alternative technique using continuous signals has emerged, requiring considerably less transmission power.

Electromagnetic waves are reflected by the ionosphere as long as the frequency of the incidence wave is below the *plasma frequency*

$$\omega_{\mathrm{pe}}^2 = \frac{n_{\mathrm{e}} e^2}{\varepsilon_0 m},$$

where n_{e} is the density of electrons, e is the electron charge, m is its mass and ε_0 is the permittivity of free space. Hence, if the frequency of the radio pulse is gradually increased, the ionosphere can be probed for both electron density *and* altitude. An ionosonde automates this process by sweeping the pulse frequency and recording the received echos in a constant cycle. The measurements are visualized in an *ionogram*, which is a plot of reflection altitude over the electron density. With the introduction of digital signal-processing, ionosondes have been greatly enhanced. Several other characteristics of the received signal such as direction of arrival as well as polarization can now be distinguished. Ionospheric echoes are circularly polarized in either O- or X-mode[4].

As visualized in figure 1.2, an ionosonde system consists of transmitter- and receiver antennas, as well as signal generation- and processing. The receiver antenna for the current ionosonde project has already been developed in another thesis project at the KTH

[3]The radar concept (**Ra**dio **D**etection **a**nd **R**anging) originates from these experiments.
[4]**o**rdinary (left-hand) or e**x**traordinary (right-hand)

Figure 1.3: The Alfvén Laboratory at the Royal Institute of Technology (KTH) in Stockholm, Sweden. ©Pictometry/Blom Swe AB.

[*Dheim*, 2008]. Since the transmission power is limited due available equipment[5], the system will use a continuous sounding signal . Furthermore, continuous sounding is much less susceptible for the interferences that are likely to exist at the antenna site.

The ionosonde is located at the Alfvén Laboratory (see figure 1.3), where the backyard of the laboratory serves as location for the transmitter antenna[6]. The yard is about 35 meters wide and about 62 meters long. It consists primarily of parking space with trees in the southwest corner and partly-subsurfaced premises in the south. The laboratory building itself consists of reinforced concrete and an outer layer of isolation material and bricks. Some parts of the roof are covered by copper or metal, other parts with common roofing

[5]The amplifier has a maximum power rating of 15 Watts

[6]The exact location is 59°20’59” N and 18°04’22” E at 44 meters over sealevel.

cardboard. A steel lattice mast is located close to the center of the backyard. This mast has a height of about 18 meters and had been used for high voltage research in the old experiment hall in the northeast corner of the building. A detailed drawing of the antenna location can be found in the appendix.

Ionospheric sounding requires transmission antennas with excessive size and bandwidth. Because transmission antennas are passive radiators, their size will range in the same order as the maximum wavelength. Furthermore, the ionosphere reflects radio waves with frequencies of up to 20 MHz, with most of the reflections occurring at frequencies between 1 and 10 MHz. All together, this gives a maximum wavelength of about 300 meters, and a bandwidth ratio of about 1:10. It is readily apparent that the antenna location does not provide the necessary space for such an antenna. However, sufficient operation down to 3 MHz was thought to be possible. Additionally, an extension of the existent mast was considered in order to provide sufficient antenna height. In order to probe for x-*and* o-mode echoes, the antenna must radiate a linear field. Alternatively, two oppositely circular-polarized antennas can be used.

In conclusion, the aim of this project was to find the optimal design of a passive antenna radiating a vertical incidence beam at frequencies between 2 and 20 MHz with either linear or circular polarization and a maximum size of 35 to 62 meters, as well as to assemble the designed structure. The following sections will discuss potential antenna types, as well as simulation and construction.

Chapter 2

Broadband Antenna Types

Various antenna types for HF bands were examined with focus on their broadband features as well as their geometry. These antenna types can be categorized into three different groups: *broadband dipoles*, *traveling wave* antennas and *frequency independent* antennas. Certain antenna types, like patch antennas, horns, parabolic- and aperture antennas as well as antenna arrays have been omitted due to their respective properties, like size or frequency response, which were found to be inadequate. Instead, the evaluation focused on typical broadband antennas and their bandwidth- and radiation characteristics, as well as their dimensions and construction.

2.1 Broadband Dipoles

Dipole antennas have low bandwidth as they are resonant radiators. However, as stated by *Balanis* [2005, p.641], "the bandwidth of an antenna (which can be closed within a sphere of radius r) can be improved only if the antenna utilizes efficiently, with its geometrical configuration, the available volume within the sphere". This requirement is satisfied to different extend by the following configurations, as shown in figure 2.1.

Cylindrical dipoles are used widely for broadcasting and communication over narrow frequency bands. As is typical for dipoles, their radiation pattern is omnidirectional and polarized along with the major axis of their structures and with considerably low gain. The bandwidth is limited as the input impedance varies with frequency [*Balanis*, 2005, p.509].

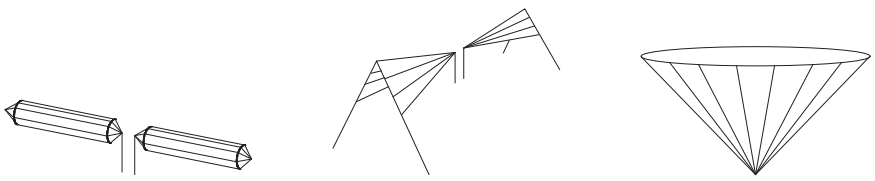

Figure 2.1: Broadband dipole antennas. (a) Cylindrical dipole. (b) Biconical dipole. (c) Conical monopole.

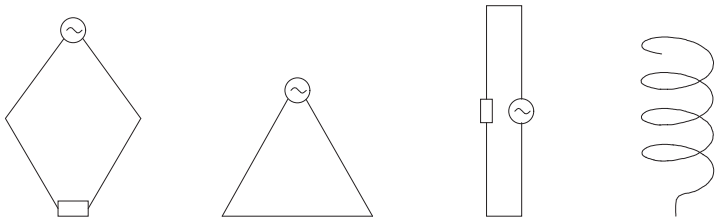

Figure 2.2: Traveling wave antennas. (a) Rhombic. (b) Delta. (c) Terminated folded dipole. (d) Helical.

Measured in wavelengths, all antenna dimensions do change with frequency – except those defined by angles. Thus, if certain geometry parameters are defined by angles, better broadband qualities can be achieved [*Balanis*, 2005, p.500]. This applies both to *biconical* dipoles and *conical* monopoles. Radiation patterns are similar to that of standard dipoles. Conical (or broadband) monopoles are commonly used for omnidirectional shortwave radio broadcasting and require a conducting ground plane.

In summary, broadband dipoles – cylindrical and biconical dipoles as well as conical monopoles – may achieve moderate bandwidths and are considerably simple structures. Their dimensions extend typically to the order of one-half wavelength, and their radiation patterns are omnidirectional with either horizontal- or vertical polarization. The pattern changes, however, as the major lobe splits at higher frequencies.

2.2 Traveling Wave Antennas

Unlike resonant radiators as the broadband dipoles in the previous section, traveling wave antennas (also called non-resonant antennas) feature a virtually uniform current pattern. This current pattern is obtained by terminating the structure properly, and thereby eliminating reflections. The antenna can be terminated by either a matching resistance, leading to certain loss if used as a transmitter, or by continuous loss due to radiation, as in case of the helical antenna. Because of their uniform current pattern, traveling wave antennas feature desireable broadband properties. Figure 2.2 shows four different configurations.

Rhombic antennas, as described by *Bruce* et al. [1935], originate from a single terminated wire – typically referred to as *beverage* antenna – and later on the *V*-antenna. Rhombic antennas consist of two wires at about one-half wavelength above ground in a rhombic shape, with the balanced feed on one end and a termination on the other end. These antennas feature horizontal polarization and one major lobe. They are among the oldest broadband antenna types and widely used for long-range broadcasting.

Top-driven *delta-* or *triangular loop* antennas feature better broadband impedance characteristics then other shapes of polygonal loop antennas, as found by *Tsukiji* and *Tou* [1980]. These antennas are made up of a simple delta-shaped loop in a vertical plane suspended on a single mast. Their omnidirectional radiation pattern is vertically polarized and has a major lobe which splits into two lobes at higher frequencies. *Tsukiji* and *Tou*

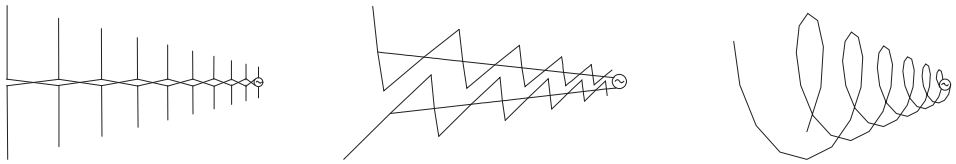

(a) (b) (c)

Figure 2.3: Frequency independent antennas. (a) Log-periodic dipole array. (b) Log-periodic zigzag antenna. (c) Conical log-spiral.

[1979] also found that the impedance characteristics of a delta antenna, although superior to other loop antennas, change rapidly over frequency. Nevertheless, delta antennas are used in many applications for ionospheric sounding.

Folded dipoles – inherently resonant radiators – exhibit a uniform current pattern if terminated properly, and by that they also gain broadband properties. Similar to their resonant counterpart, terminated dipoles radiate an omnidirectional field, polarized in parallel to the main axis of the antenna. For ease of construction, these antennas are often suspended from a mast or building to ground, and are therefore very popular among radio amateurs [*Cebik*, 2000; *Coro*, 2007].

Helical antennas achieve a uniform current pattern due to radiation loss [*Kraus* and *Marhefka*, 2002, p.225]. They consist of a wire wound in a helical shape, extending from a ground plane with the feed point between the plane and the wire. Depending on the size of the structure with respect to the wavelength, helical antennas operate in either the normal- or the axial (end-fire) mode. In the normal mode, the antenna is much smaller than the wavelength, and the radiation pattern resembles that of a small loop. In the axial mode, the antenna radiates an endfire pattern with circular polarization. Because of their circular polarization, helical antennas are used commonly as ground station antennas for satellites and spacecrafts.

In summary, traveling wave antennas attain broadband properties to various extent, ranging from the helical and delta antennas with rather moderate bandwidth to the terminated-folded dipole and rhombic antennas with large bandwidth. Antenna dimensions span from one wavelength in circumference for the delta and helical antennas up to several wavelengths for the rhombic. Radiation patterns are either omnidirectional as for the delta- and dipole antennas or focused into one lobe as for the helical and rhombic antennas. Although fairly simple in geometry, traveling wave antennas are considerably large structures with a certain construction effort.

2.3 Frequency Independent Antennas

In the concept of frequency independent (FI) antennas by *Rumsey* [1957], periodic structures, which vary with the logarithm of the frequency, are described. Although absolutely frequency-independent in theory (extending infinitely in space), these antennas are limited in bandwidth due to inevitable physical truncation. Nonetheless, very large bandwidths can

be achieved. A complete survey over FI antennas has been presented by *Mayes* [1992]. Figure 2.3 shows three different types of FI antennas.

Conical log-spiral (CLS) antennas, developed by *Dyson* [1959a,b], are made up of two arms of electric wire rotated at a constant angle around an imaginary cone with the feed connected to both arms. Current patterns along these arms are steadily decreasing due to radiation loss (one might consider the CLS as a travelling wave antenna), with a so called *active region* of major radiation. With decreasing frequency, this active region moves away from the cone apex. The radiation pattern is circular-polarized with a major lobe in direction of the cone apex.

Log-periodic zigzag antennas (LPZZ) and *log-periodic dipole arrays* (LPDA) originate from advancements in FI antennas and the demand for a linear-polarized broadand antenna [*DuHamel* and *Isbell*, 1957; *DuHamel* and *Ore*, 1958]. LPZZ antennas contain two planes of logarithmically-spaced zigzag-wire each fed by a single wire along the plane center with a balanced feed at the apex [*Bell* et al., 1960]. LPDAs, as developed by *Isbell* [1960], evolved from the same roots as the LPZZ, but consist of a number of half-wavelength dipoles. These dipoles vary log-periodically in length and distance from the apex and are fed by a transmission line in a phase-alternating manner. The LPDA can be considered as a LPZZ with an apex angle of zero degrees and straight elements.

Both LPZZs and the LPDAs radiate from just a small number of elements. This active region (similar to the CLS) moves along the antenna with frequency and dissipates all power from remaining elements. These antennas have a horizontal-polarized radiation pattern with a major endfire lobe in direction of the antenna apex.

In a short summary, FI antennas have superior broadband capabilities and are limited by their physical size only. Lower- and higher frequency limits are determined by maximum- and minimum element length or diameter respectively. Both circular and linear polarization can be attained, as well as narrow radiation lobes with high gain. However, all FI antennas are complex structures and need precise calculation as well as construction.

Chapter 3

Antenna Design

Following the antenna survey in the previous chapter, broadband- and geometry properties of the different antenna types were matched against the requirements stated in section 1.2. It was found that a majority of the dipole- and traveling-wave antenna types do not offer the required broadband features. Although some, like the biconical dipole and the rhombic antenna might perform well over wide frequency spans, their size as well as their radiation patterns were found to be deficient. Eventually, the frequency independent antennas were chosen for more detailed analysis because of their superior broadband capabilities as well as their feasible size.

For this detailed analysis, computer models were produced and simulated in order to identify the effects of several geometric parameters on antenna performance. As a figure of merit, the input resistance (the real part of the input impedance) was chosen. This value consists primarily of the radiation resistance and is therefore a good measurement for radiation performance. Furthermore, impedance variations over the frequency band should be minimized. Hence, the standard deviation and mean of the input resistance were analyzed as a function of model parameters.

For the purpose of comparison, major antenna parameters were scaled to a factor of the maximum design wavelength, $\lambda_{\max}$[1].

3.1 Simulation Program

All simulations were computed with the Numerical Electromagnetics Code in version 2 (NEC2), developed by G. J. Burke and A. J. Poggio around 1980[2] at the Lawrence Livermore National Laboratory in California, USA. The code calculates a numerical solution of integral equations for induced currents[3]. Models are made up of thin wires divided into a certain number of segments. NEC2 is originally written in Fortran and has been ported to the C and C++ programming languages. It has been released for public use as source

[1] $\lambda_{\max}$ is given by the lowest design frequency; at 2 Mhz, $\lambda_{\max} \simeq 150$ m.
[2] The first version of this program dates back to the 1970s.
[3] This numerical computational method is also known as the *boundary element method* or *method of moments*.

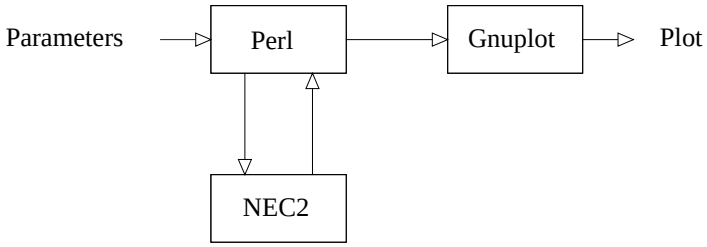

Figure 3.1: Visualization of the simulation procedure.

package and binary executable for most computing platforms[4]. The program is also known to produce highly accurate results.

But since the code utilizes some approximations, great care must be taken while writing NEC2 models [*Richeson*, 1996, p. 7]. Some fundamental modeling rules regarding segment length, Δ, and wire radius, a, related to the wavelength, λ, are listed here.

- $\Delta < 0.1\lambda$ ($\Delta < 0.05\lambda$ in critical regions)
- $\Delta > 0.001\lambda$ (To avoid numerical inaccuracy)
- $\Delta/a > 8$ ($\Delta/a > 2$ for extended kernel)
- $(2\pi a)/\lambda \ll 1$
- Segments must intersect at their end

It is also essential to avoid very sharp angles and not to vary Δ extensively over adjacent segments. Additionally, it is recommended that closely-spaced wires should be segmented equally.

Simulation of broadband antennas over great frequency-sweeps intensifies the demand for thorough segmentation. Furthermore, the complexity of these antennas necessitates a large number of segments to fulfill the modeling guidelines stated earlier. However, since radiating regions are sized according to the actual wavelength, the segmentation might vary along the model and thereby decrease complexity and computation time. Numerous simulations of different broadband antennas have shown that this flexible way of segmentation is not compromising result accuracy. Hence, it was used for all subsequent simulations.

NEC2 reads and writes ordinary text-files, and it requires all input to be formated in a strict manner of rows and columns[5]. Various programs – both commercial and free – are available to ease model generation and result visualization. But these programs were found to be inadequate for generating complex structures as used in this study. Consequently, a script for model generation, verification, parameter sweeping and output visualization has been programmed (see fig. 3.1). It is written in *Perl*, a general-purpose programming language.

[4]For this study, nec2++ Linux executable version 1.0.4 was used.
[5]In the 1970s, all code was fed into computers on so called *punch cards*.

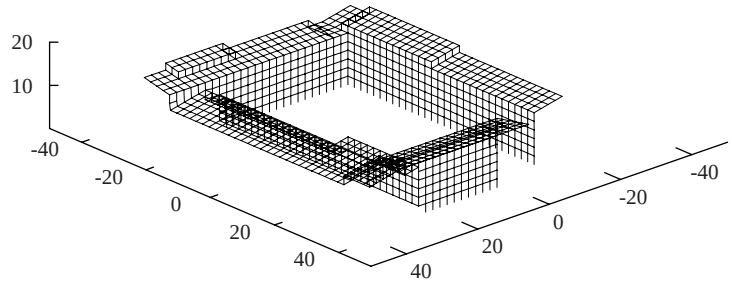

Figure 3.2: Wire model of the Alfvén Laboratory building composed of 4567 segments in a mesh-spacing of 1 m and a wire diameter of 5 mm. The model is centered to mast position and viewed from 30° north with 25° elevation.

The script calculates wire end-points and segmentation from a mathematical description of the antenna. Wires, sources, transmission lines, loads as well as simulation parameters are then verified against model guidelines and written to an input file. The simulator is executed with that file, and writes all result data to an output file. Thereafter, the script reads the output file and writes tabular data as well as plot instructions into text files. The procedure might iterate over a certain parameter sweep. The data is then plotted with the command-line driven plotting utility *Gnuplot*.

All simulations were computed on different nodes of the KALK[6] computer cluster. These computers are equipped with 3.4 GHz Pentium 4 processors and 1 GB RAM. Simulation running-times varied from seconds to several hours or days, depending on the number of segments as well as frequency and parameter stepping. For example, a simulation of a model with 400 segments over 100 frequency steps and 50 parameter steps could take about one hour.

3.2 Surrounding and Ground

In order to determine the effect on antenna performance, structures in close vicinity to the assembly have been modeled and simulated together with a half-wavelength dipole. Although definite electrical properties are not known, the surrounding building has been emulated as a wire-grid model, displayed in figure 3.2. Simulations have shown a slight effect on radiation patterns (see figure 3.3), but no significant change in input impedance. Due to high computational load, all subsequent simulations were conducted without the Alfvén Laboratory model.

Antenna performance is also heavily affected by the existence of ground in close vicinity. Conducting surfaces, such as ground, reflect electromagnetic waves causing a mirror

[6] **K**ALK, **A**lfvénlaboratoriets **L**inux **K**luster

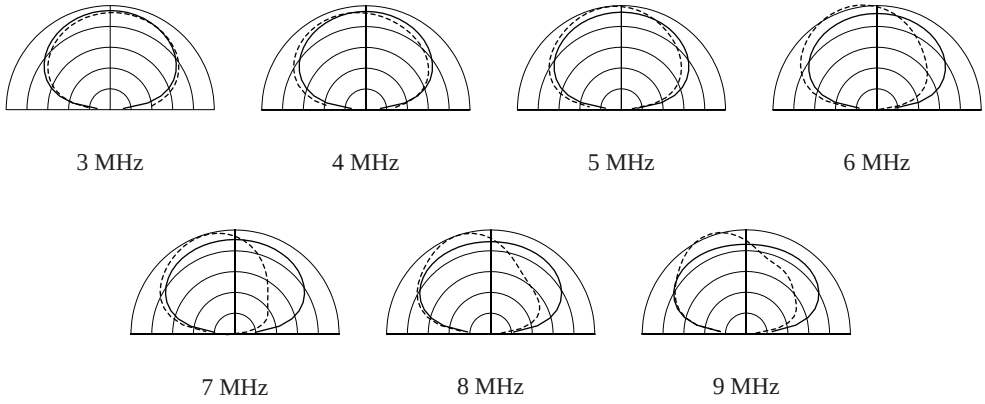

Figure 3.3: Radiation patterns in vertical plane for a half-wavelength dipole over perfect ground with (dashed line) and without (solid line) surrounding buildings. Rings marking total gain at -10, -5, 0, 5 and 10 dBi. Dipole length = $\lambda/2$, height = 10 m, wire diam. = 2 mm.

image which interacts with the antenna. This image is attenuated depending on surface conductivity, σ, whereas its position is modulated by the relative dielectric constant of the surface, ε_r. The ground at the antenna site is made up of a parking lot as well as minor partly-subsurfaced premises. Since no distinctive parameters are known and no measurements concerning the electric ground properties have been carried out, approximate values for simulation purposes were used[7].

Given accurate parameters, ground reflection can be incorporated into the antenna design and even improve antenna performance. This is usually true for structures larger than one-hundred meters. However, such accurate ground parameters do not exist for the current project, and environmental conditions – such as humidity and parking cars – are likely to alter ground properties. Therefore, focus was on designs *insensitive* to ground reflection.

3.3 Log-periodic Dipole Array

The log-periodic dipole array (LPDA) was modeled according to the basic equations given in figure 3.4. Apex angle, α, and geometric ratio, τ, were calculated from array size and number of elements respectively. Transmission-line impedance was set to 300 Ω. The antenna site allows element lengths of up to seventy meters. This yields a low-frequency limit of about 2.15 MHz for a half-wavelength dipole array.

In order to maximize element length, the array might be folded along the transmission-line, turning the two-dimensional array into a three-dimensional structure. Simulations showed that this has no negative impact on antenna impedance as long as the folding angle

[7] σ = 2 mS/m and ε_r = 5, NEC2 Sommerfeld/Norton method

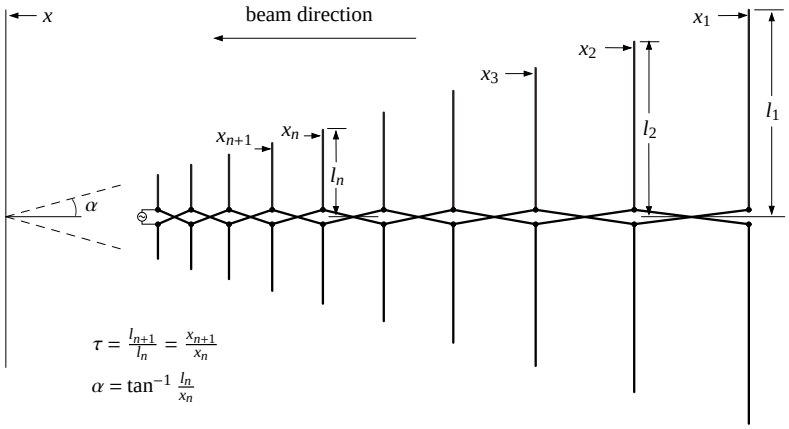

Figure 3.4: Geometry of an Log-periodic Dipole Array as described by *Isbell* [1960, p.262].

is greater than one-hundred degrees. With decreasing folding angle, the main lobe moves away from main axis.

Wire segmentation for the LPDA is described by *Cebik* et al. [2007, p.10-3]. Every dipole element is connected to a centered transmission line and should hence hold an odd number of segments. The number of segments on every subsequent element is determined by the geometry ratio, τ. However, as mentioned in section 3.1, a more flexible way of segmentation was applied for this study. Every dipole element was given the same number of segments, thereby reducing the total number of segments. It was found that this new, flexible, segmentation procedure is able to reduce simulation time significantly without compromising result accuracy.

As discussed in the previous section, ground reflections were not incorporated into the current antenna design. This implies an apex-up design, since the LPDA has end-fire ra-

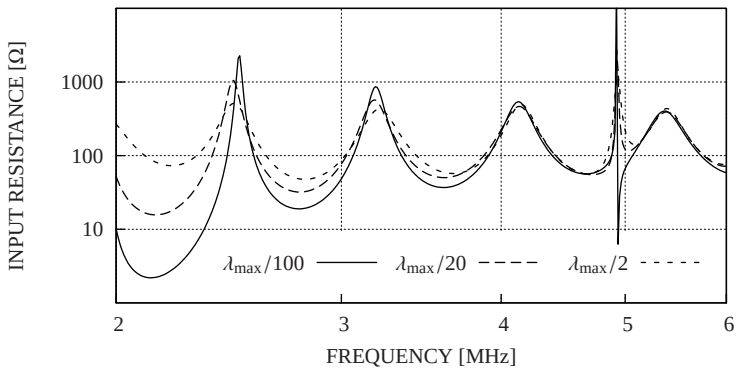

Figure 3.5: Input resistance for an LPDA at different distances to perfect ground with $W = \lambda_{max}/2$, $w = \lambda_{min}/2$, $H = \lambda_{max}/6$, $\alpha = 56°$, $\tau = 0.77$, wire diam. $= \lambda_{min} \cdot 10^{-4}$.

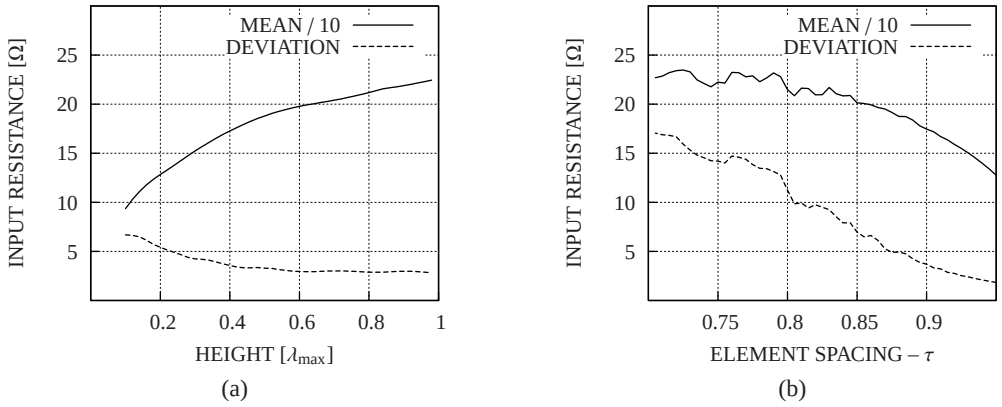

Figure 3.6: Standard deviation and arithmetic mean of input resistance for an LPDA as a function of (a) antenna height, and (b) antenna element spacing with $W = \lambda_{max}/2$, $w = \lambda_{min}/2$, $H = \lambda_{max}/2$, $\alpha = 56°$, $\tau = 0.89$, wire diam. $= \lambda_{min} \cdot 10^{-4}$, free space, at 3 to 9 MHz.

diation characteristics. Nevertheless, both apex-up and apex-down designs were simulated over ground, revealing minor advantages for the apex-up design.

The input resistance varies heavily over frequency, as plotted in figure 3.5. These variations come from the limited frequency span covered by a single dipole, as well as couplings between the array and its ground image. With decreased ground distance and lower frequency, more variations can be seen. The pattern in figure 3.5 shows also a glitch at around 5 MHz, which is caused by resonances on elements outside the active region. These resonances occur when the active region is underpopulated at a certain frequency. But the resonances are also caused by interactions between the array and its ground image.

Height and element-spacing were varied over multiple simulations in order to distinguish the influence of these parameters on antenna performace. In figure 3.6, the results of these simulations are summarized as standard deviation and arithmetic mean of the input impedance over a frequency span from 3 to 9 MHz. Since antenna height is limited, undesirable deviation – and a particular lower mean – cannot be avoided, even if element spacing is minimized.

3.4 Conical Log-Spiral Antenna

The basic parameters associated with the conical log-spiral (CLS) are shown in figure 3.7. Given antenna height, H, base diameter, B, and pitch angle, ξ, wire positions were calculated with the following equations [*Dietrich* and *Long*, 1969].

$$\rho = R_{max} e^{-a\tau}$$

$$a = \tan\xi \sin(\psi/2)$$

Starting at base level ($\rho = R_{\max}$), succeeding wire points are given by increasing rotation angle, τ. Furthermore, a two-arm configuration was found to be the most adequate among several options [*Sivan-Sussman*, 1963, fig. 7, p. 536]. As common for this frequency region, a constant arm width (wire diameter) simplifies construction additionally. However, since the fundamental design by *Rumsey* specified expanding spiral-arms, this constant-arm CLS can no longer be considered as a frequency independent antenna.

A rather simplistic segmentation procedure, as outlined in section 3.1, was applied. Every wire, disregarding its length, was given the same number of segments. Current patterns along the spiral arms, compared to results reported by *Yeh* and *Mei* [1967, Fig. 8, p. 638], indicated sufficient model accuracy.

In order to simplify constrution as well as to improve antenna performance for the given antenna site, the original circular design was modified. By increasing rotation-angle step-width, $\Delta\tau$, between adjacent wire points, the circular base of the spiral is reduced to a polygonal – and ultimately – a rectangular shape. The result is a *pyramidal* spiral, which is not only easier to construct, but also holds a lower cut-off frequency since its circumference is larger in respect to that of its circular counterpart on the same quadratic base. Furthermore, *Tang* [1963, p.427] shows that this design performs almost as good as a standard circular cone. Therefore, all subsequent simulations focused on the pyramidal log-spiral (**PLS**).

Proceeding the assessments of section 3.2, an apex-up design for the PLS was chosen. Moreover, the apex-up configuration exhibits much less construction effort than the

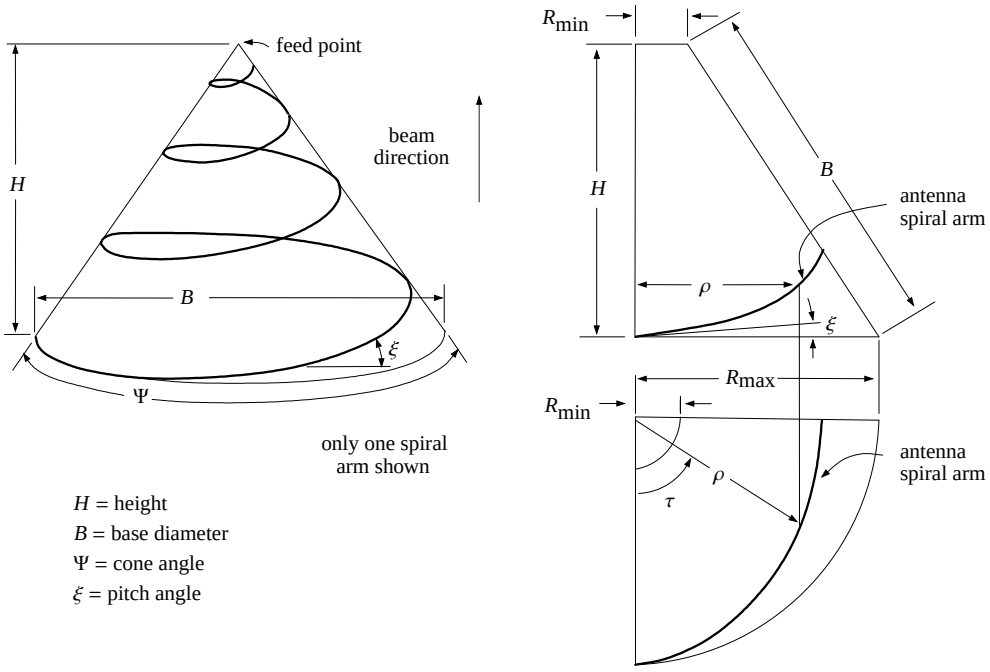

Figure 3.7: Geometry of a conical log-spiral as shown by *Dietrich* and *Long* [1969, p.552].

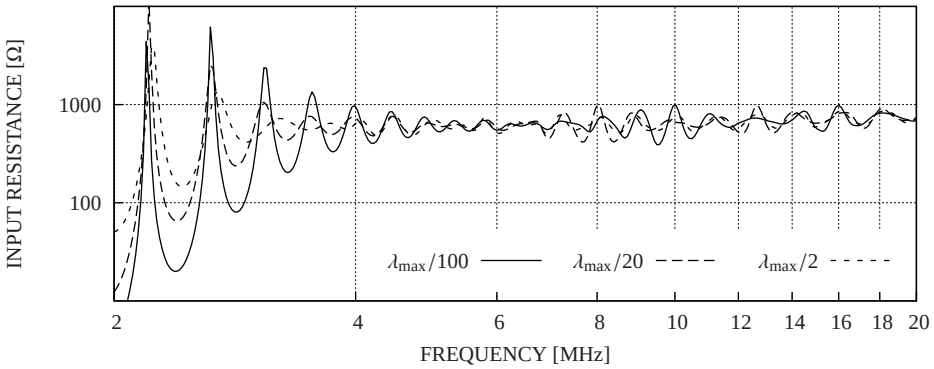

Figure 3.8: Input resistance for a pyramidal log-spiral antenna at different distances to perfect ground with $H = \lambda_{max}/6$, $B = \lambda_{max}/3$, $R_{min} = \lambda_{min}/10$, $\xi = 5°$, wire diam. $= \lambda_{min} \cdot 10^{-4}$.

apex-down design for antennas this size [*Xiaorong* et al., 2000, p. 27]. However, similar to LPDAs, the apex-up PLS is sensitive to ground reflection at low- as well as medium frequencies (see figure 3.8).

The base plane available at the antenna site can be utilized to an even greater extent by reducing the ratio between length and width of the rectangular base. *Cathey* and *Beck* [1964] studied a related modification of a circular spiral on an elliptical cone with promising results. However, such modifications affect input impedance characteristics of the PLS, as shown in figure 3.9a.

As for the LPDA, the feasible antenna height for the PLS is well below optimum. This affects not only input properties, as shown in figure 3.9b, but also radiation patterns (decreased beam width). In order to differentiate antenna height from other variables, expansion rate, a, – and thereby the spiral arm length – has been held constant during these simulations. With decreased antenna height (and thereby increased cone angle, Ψ), spiral arm-length – and consequently all other antenna characteristics – become very sensitive to expansion angle, ξ. As this angle narrows down, the active regions become more dense and impedance variations abate (see figure 3.9c).

Wire- and feed diameters control primarily mean input-resistance, as presented in figures 3.9d and 3.9e. These results are consistent with the assessments by *Dyson* [1965, p.496], if one considers the wire diameter as being closely related to the angular arm width. Steps in the feed-diameter graph are caused by the model generation procedure, where the structure is built until a certain feed-diameter is exceeded.

Low-frequency operation is limited by the base diameter of the PLS. As frequency declines and the active region moves against the open end of the PLS, currents along the spiral arms are reflected at the wire endings. To reduce these reflections, the antenna can be loaded with either a resistor [*Hertel* and *Smith*, 2002, p.27, fig.3] or several turns of wire, as analyzed by *Yang* and *Iizuka* [1983, p.349] as well as by *Dietrich* and *Long* [1969, p.553]. The latter modification, however, was difficult to simulate due to the restrictions of

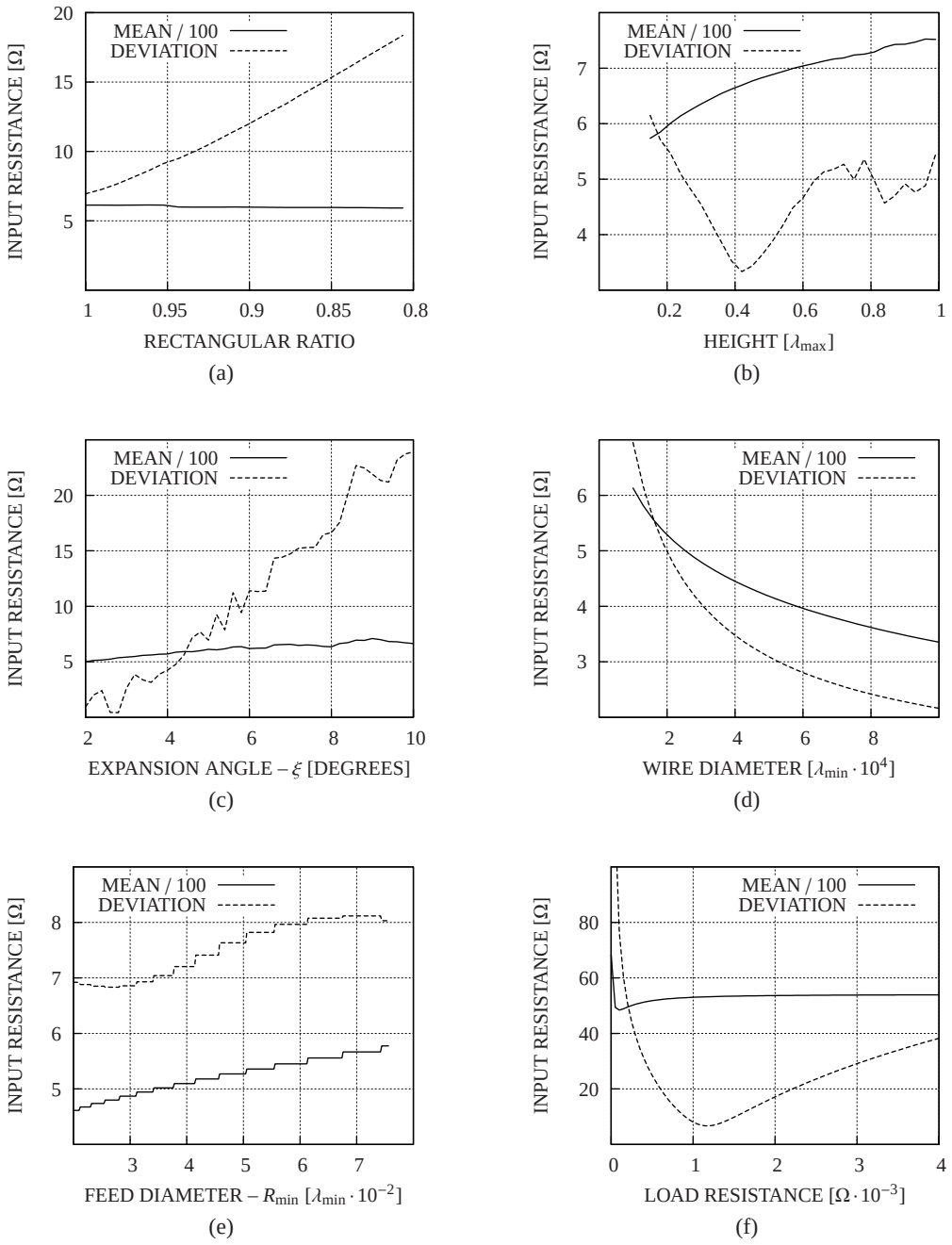

Figure 3.9: Standard deviation and arithmetic mean of input resistance for a pyramidal log-spiral antenna as a function of (a) rectangular ratio, (b) height at constant expansion rate a, (c) expansion angle ξ, (d) wire diameter, (e) feed diameter, and (f) load resistance with $B = \lambda_{max}/3$ and, if not varied, $H = \lambda_{max}/6$, $R_{min} = \lambda_{min}/10$, $\xi = 5°$, wire diam. $= \lambda_{min} \cdot 10^{-4}$, $R_{load} = \infty$, free space, rect. ratio = 2, at 3 – 9 Mhz, and in (f) at 1 – 4 MHz.

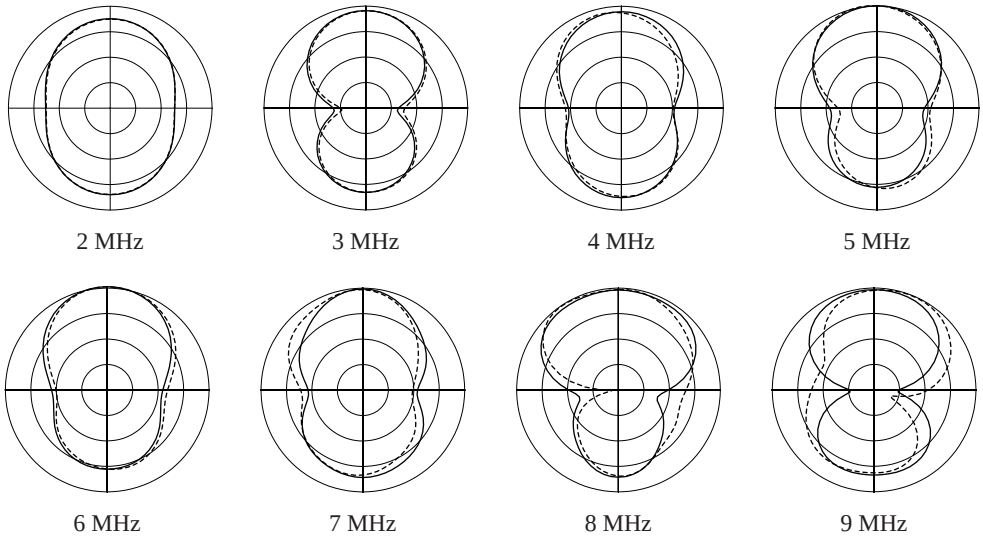

Figure 3.10: Radiation patterns in vertical plane for a pyramidal log-spiral antenna with the cone apex centered (solid line) and at $\lambda_{max}/6$ from center (dashed line). Rings marking total gain at -10, -5, 0 and 5 dBi. $H = \lambda_{\max}/6$, $B = \lambda_{\max}/3$, $R_{\min} = \lambda_{\min}/10$, $\xi = 5°$, wire diam. $= \lambda_{\min} \cdot 10^{-4}$, free space.

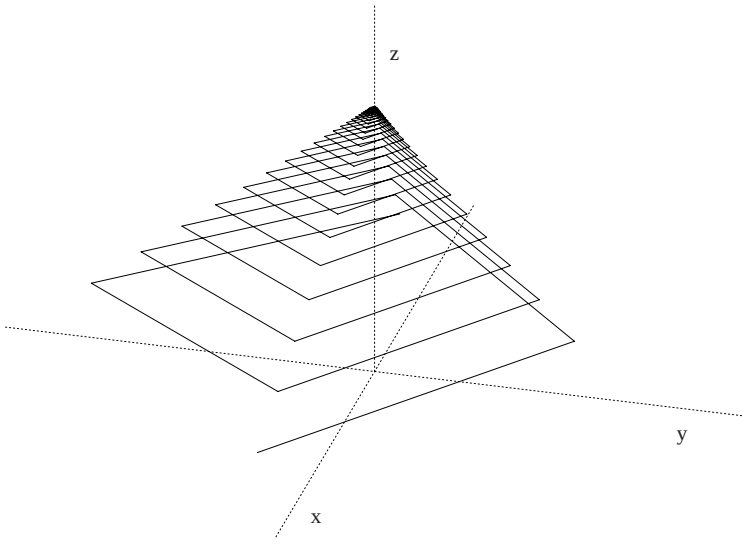

Figure 3.11: Wire model for the optimized pyramidal log-spiral antenna as in figure 3.12.

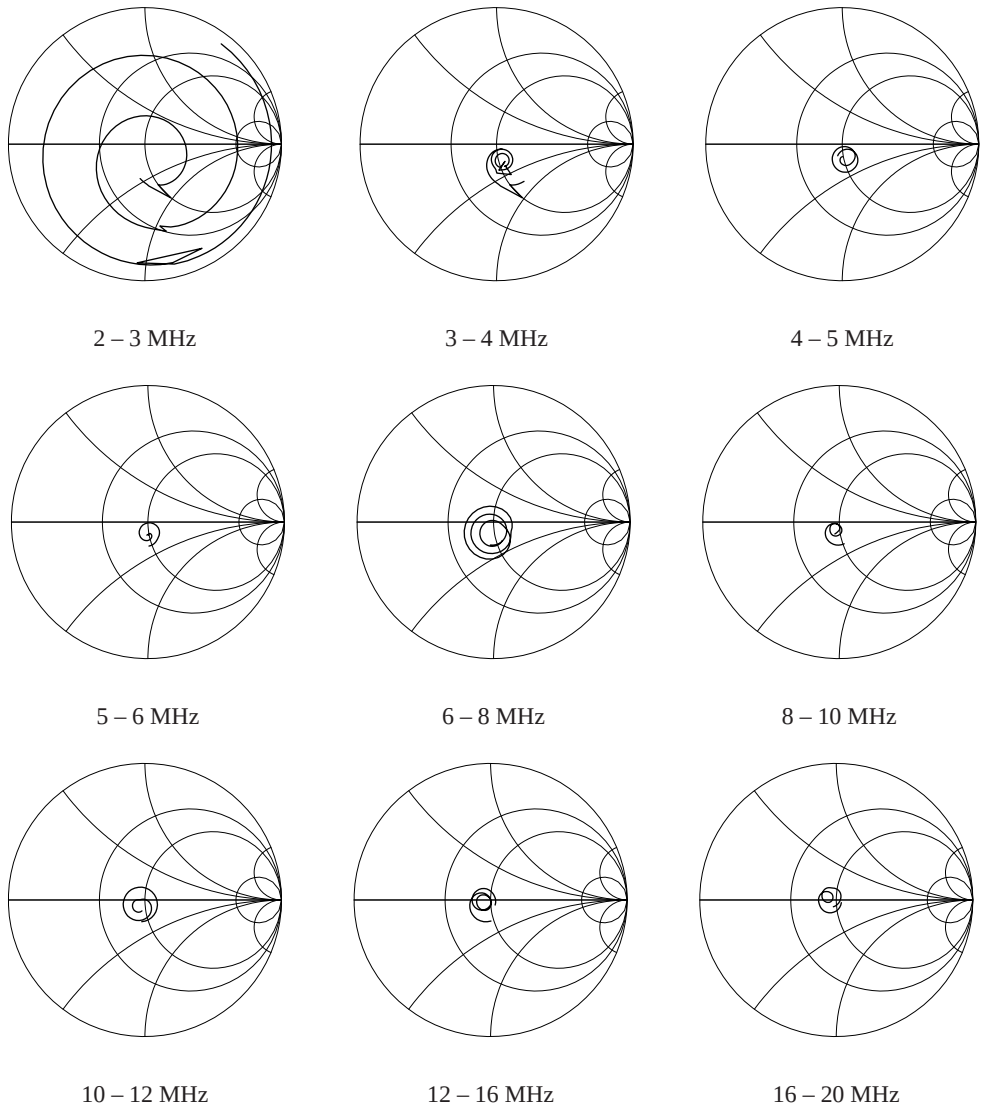

Figure 3.12: Smith-chart representation of the input impedance for the optimized pyramidal log-spiral antenna. H = 25.63 m, B = 50.43 m, R_{min} = 0.3 m, $\xi = 5°$, wire diam. = 1.63 mm, $R_{\text{load}} = \infty$, height over ground = 10.65 m, σ = 2 mS/m, ε_{r} = 5, x-position = 9.263 m, y-position = -1.951 m, $Z_0 = 450\ \Omega$.

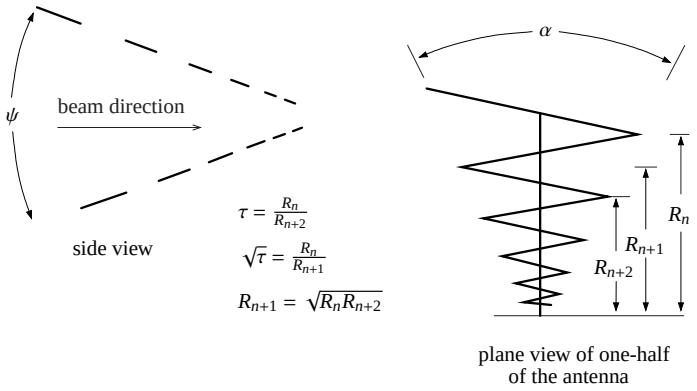

Figure 3.13: Geometry for the log-periodic zigzag antenna as shown by *Bell* et al. [1960, p.560].

NEC2 concerning long closely-spaced wires. Nevertheless, the effect of resistive loading was simulated and is displayed in figure 3.9f.

Since the supporting mast at the antenna site is not centered on the antenna base plane, the pyramid apex is dislocated. This alteration to the original design has negligible impact on input impedance. However, as shown in figure 3.10, radiation patterns are slightly diverted at higher frequencies.

All preceding design parameters were optimized to the current antenna location through numerous simulations. The model of the final design is shown in figure 3.11, and a Smith chart representation of its input impedance over the desired frequency band can be found in figure 3.12. Some irregularities in the first two Smith charts are caused by strong resonances on the antenna.

3.5 Log-periodic Zigzag Antenna

The log-periodic zigzag antenna (LPZZ) is displayed in figure 3.13, together with corresponding parameters and design equations. Plane angle, α, and apex angle, Ψ, are given by base-plane- width, W, and length, L, as well as antenna height, H. Adjacent wire points were calculated with the geometric ratio, τ, starting at base level and then moving along the zigzag plane towards the plane apex, until the tooth-length falls below half of the shortest element length, $w/2$. All models used a constant wire diameter.

Triangular tooth-structures, although further away from the original frequency independent configuration, perform as good – if not better – as trapezoidal tooth-structures [*DuHamel* and *Ore*, 1958, p.147]. They are also easier to construct. Another design option – a bent zigzag antenna as described by *Greiser* and *Mayes* [1964] – features lower frequency limits than standard zigzag antennas. For this option, the zigzag plane is bent at a right angle along the feedline, providing twice the tooth length on the same quadratic antenna base. However, since the antenna location is a rectangular base with a ratio of almost 1 to 1.75, only a minor tooth extension (at a much higher construction effort) is possible.

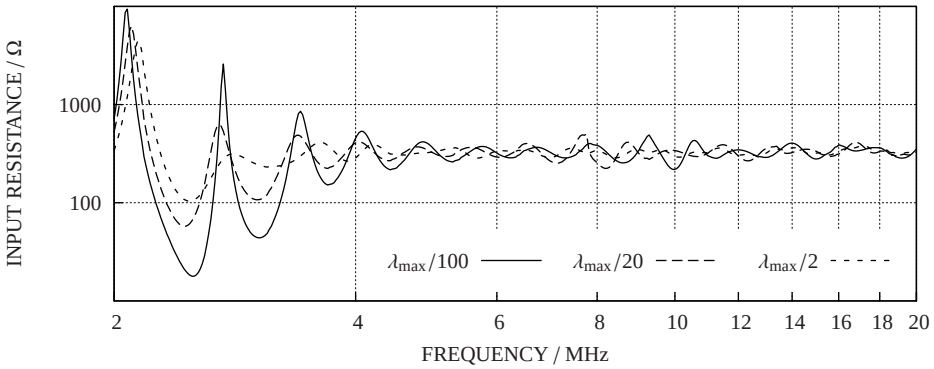

Figure 3.14: Input resistance for a log-periodic zigzag antenna at different distances to perfect ground with $W = \lambda_{max}/2.5$, $\Psi = 36°$, $w = \lambda_{min}/3$, $H = \lambda_{max}/6$, $L = \lambda_{max}/4$, $\alpha = 88°$, $\tau = 0.7$, wire diam. $= \lambda_{min} \cdot 10^{-4}$.

Therefore, the standard zigzag configuration was chosen.

Following the concept of a more flexible segmentation (see section 3.1), three different segmentation procedures for the LPZZ were developed. The first method defines the maximum segment-length, Δ_{max}, as

$$\Delta_{max} = \lambda \cdot \text{segmentation ratio.}$$

This produces models with fewer segments for low- and mid-range frequencies. However, Δ varies rather extensively over adjacent segments, especially around the center feedline. The second method on the other hand minimizes these segment-length variations by segmenting the tooth wires according to the corresponding feed wire-length.

$$\Delta_{tooth} \simeq \Delta_{feed}$$

Additionally, such models do not change with frequency and yield very low segment densities. For the third method, Δ_{max} is given by the length of the shortest feed segment.

$$\Delta_{max} = \Delta_{feed_{min}}$$

As the previous one, this method does not depend on frequency and features even lower segment-length variations. However, it might produce very high segment-densities for antennas with short elements. Simulations revealed no significant difference between these three methods. Therefore, the procedure with the lowest segmentation rate – method two – was used for all subsequent simulations of the LPZZ.

As for the PLS, the impact of ground reflection on the performance of the LPZZ was given serious consideration. In response to the close coupling between the antenna and its ground image, *Grubb* and *Jones* (personal communication, “The search for the ideal vertical incidence broadband HF antenna” by R. N. Grubb and J. E. Jones, 1981) proposed an apex-down configuration. However, due to the uncertain ground parameters discussed

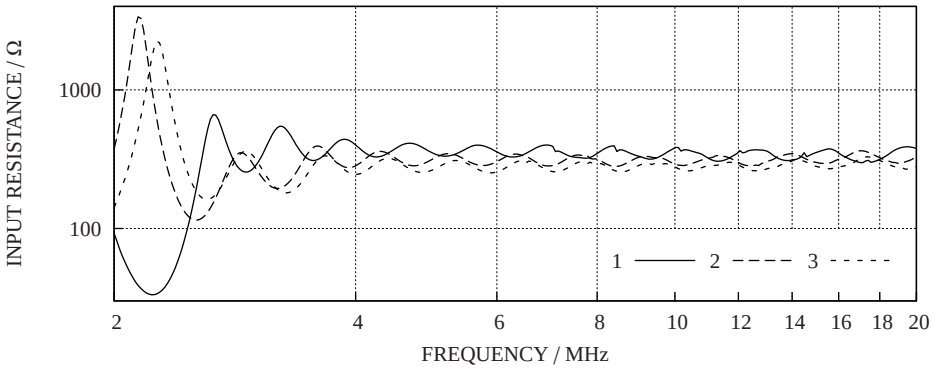

Figure 3.15: Input resistance for a log-periodic zigzag antenna with one, two or three feedwires. $W = \lambda_{max}/2.5$, $\Psi = 36°$, $w = \lambda_{min}/3$, $H = \lambda_{max}/6$, $L = \lambda_{max}/4$, $\alpha = 88°$, $\tau = 0.7$, wire diam. $= \lambda_{min} \cdot 10^{-4}$, free space

in section 3.2, an apex-up design was chosen. Simulations revealed that ground reflections are, as for the PLS, most severe at lower frequencies. But even mid-range frequencies are affected, as seen in figure 3.14.

Three different feed arrangements do exist for the LPZZ. The first, a triangular feed boom, is consistent with the requirements of a frequency independent design since the feed width varies with expanding zigzag dimensions. This triangular feed boom might consist of two or three feed wires. Feed connection points are calculated utilizing the following equation [*Lee* and *Mei*, 1970, p.761].

$$\text{Tooth angle} = 180° - 2\cot^{-1}\left[\frac{4\sigma}{(1+\tau^{1/2})^2}\right],$$

where

$$\sigma = \left(\frac{1-\tau}{4}\right)\cot\left(\frac{\alpha}{2}\right).$$

For the second arrangement, the feed angle is decreased to zero, leaving the antenna with a single feedwire [*DuHamel* and *Ore*, 1958, p.144]. This simplifies construction substantially. The last option is to discard the feed-boom entirely, which leads to a complete different antenna configuration than the original zigzag design. Simulations indicated also that this design lacks the frequency independent performance common to the zigzag antenna, and it was therefore discarded. The remaining feedwire configurations differ very little in performance, as can be seen in figure 3.15. As readily apparent, the number of feedwires affects mainly the mean input resistance. The two-wire feed design is very similar to its three-wire counterpart, yet easier to construct. However, final optimizations revealed a slight advantage in standing wave ratio for the single feedwire version over its triangular counterpart.

Several other design parameters have been examined in more detail. As can be seen in figure 3.16a, the LPZZ reacts more settled on element spacing then the PLS, and it shows

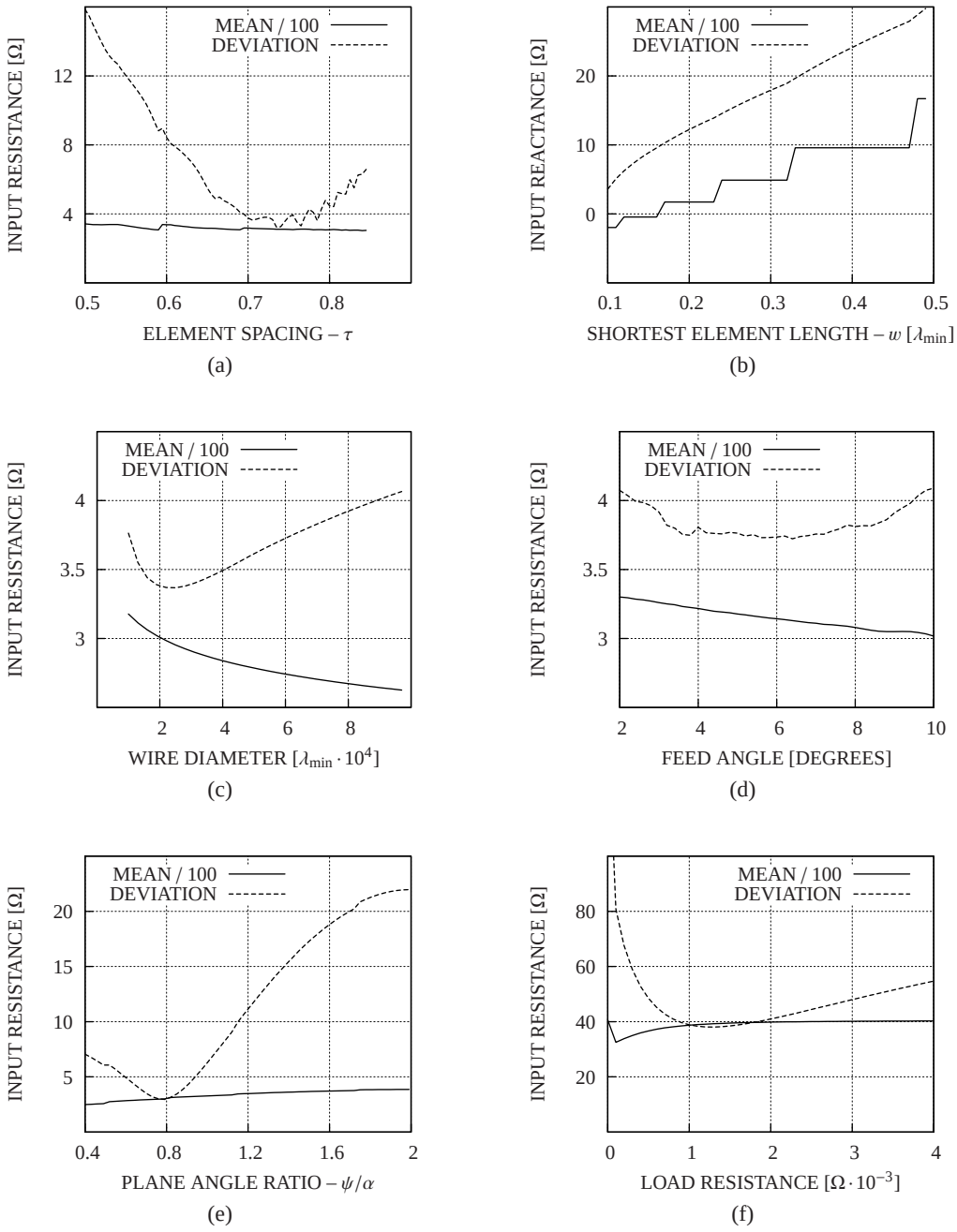

Figure 3.16: Standard deviation and arithmetic mean of input resistance for a log-periodic zigzag antenna as a function of (a) element spacing τ, (b) shortest element length w (graph shows input reactance), (c) wire diameter, (d) feed angle, (e) plane angle ratio and (f) load resistance with $W = \lambda_{max}/2.5$, $\Psi = 36°$, $w = \lambda_{min}/3$, $H = \lambda_{max}/6$, $L = \lambda_{max}/4$, $\alpha = 88°$, $\tau = 0.7$, wire diam. $= \lambda_{min} \cdot 10^{-4}$, free space at $f = 3 - 9$ Mhz; in (e) at $f = 1 - 3$ MHz.

a distinctive optimum at around 0.75. The length of the shortest element, w, is not only determining the upper frequency limit, but has also great influence on the imaginary part of the input impedance, as can be seen in figure 3.16b. Although an upper frequency limit at about 15 - 20 MHz would be sufficient, a much smaller w was chosen. In consistency with the results for the PLS, the wire diameter affects mainly the mean input resistance and has only a minor impact on the input-resistance deviation (see figure 3.16c). The angle for feed arrangements of two or more feedwires was varied, and the results are shown in figure 3.16d. Any affect on the standing wave ratio, as reported by *Grubb* and *Jones* (same personal communication, p.5), may be explained by the change in mean resistance. The ratio between apex angle, Ψ, and plane angle, α, as shown in figure 3.16e, was of higher interest then antenna height. Fortunately, the optimal ratio (about 0.8) is close to the real conditions at the antenna site.

Improving the low-frequency response of the LPZZ proved to be difficult. In order to radiate at lower frequencies, the longest antenna element might be extended beyond the original zigzag structure towards the second curtain. However, this modification was not found to be beneficial, no matter in which direction the wire extended.

Similar to the PLS, a resistive loading of the LPZZ was examined. Instead of one wire span holding the resistance between both zigzag ends, two separate load wires between zigzag ends and the ground plane were modeled. This loading had not the same remarkable effect as for the PLS, but might provide a medium standing wave ratio for frequencies just

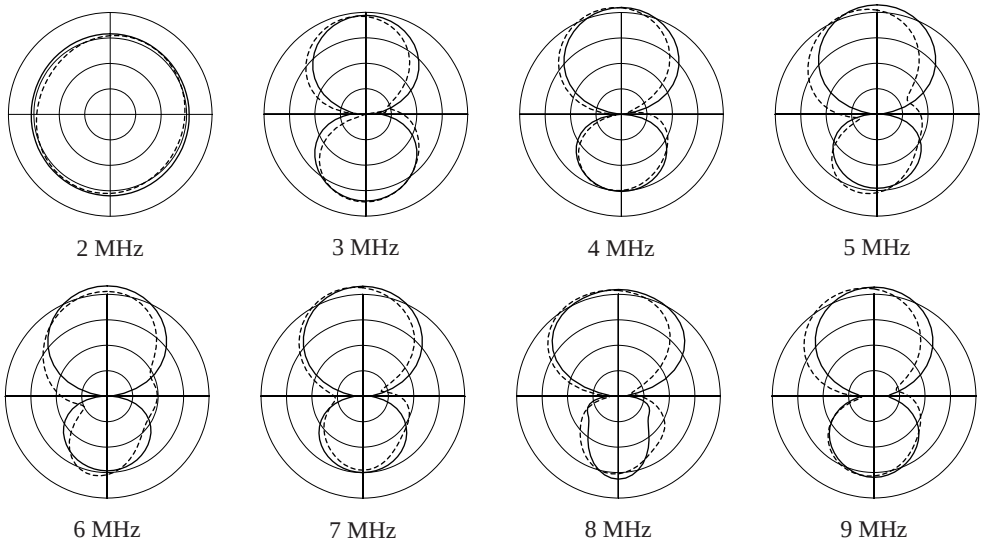

Figure 3.17: Radiation patterns in vertical plane for a log-periodic zigzag antenna with the plane apex centered (solid line) and at $\lambda_{max}/10$ from center (dashed line). $W = \lambda_{max}/2.5$, $\Psi = 36°$, $w = \lambda_{min}/3$, $H = \lambda_{max}/6$, $L = \lambda_{max}/4$, $\alpha = 88°$, $\tau = 0.7$, wire diam. $= \lambda_{min} \cdot 10^{-4}$, free space. Rings marking total gain at -10, -5, 0 and 5 dBi.

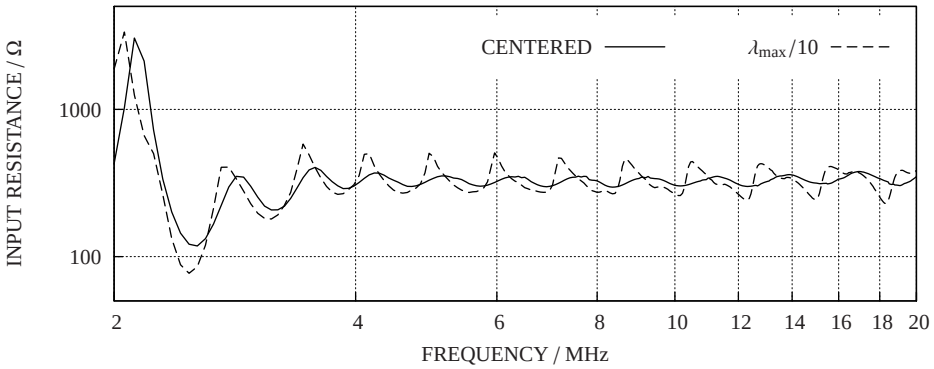

Figure 3.18: Input resistance for a log-periodic zigzag antenna as in figure 3.17.

below 2.5 MHz (see figure 3.16f). Since the LPZZ is not a true traveling-wave antenna, its low-cut frequency cannot really be improved.

Another topic of study was the impact of a shift of the antenna apex on antenna performance. Similar to the results for the PLS, radiation patterns show minor deviations (see figure 3.17). But in contrast to the spiral, the input resistance pattern is also affected, as shown in figure 3.18. This behavior was unexpected since both the LPZZ and the PLS are complementary along their vertical axes. However, the LPZZ contains feed lines which

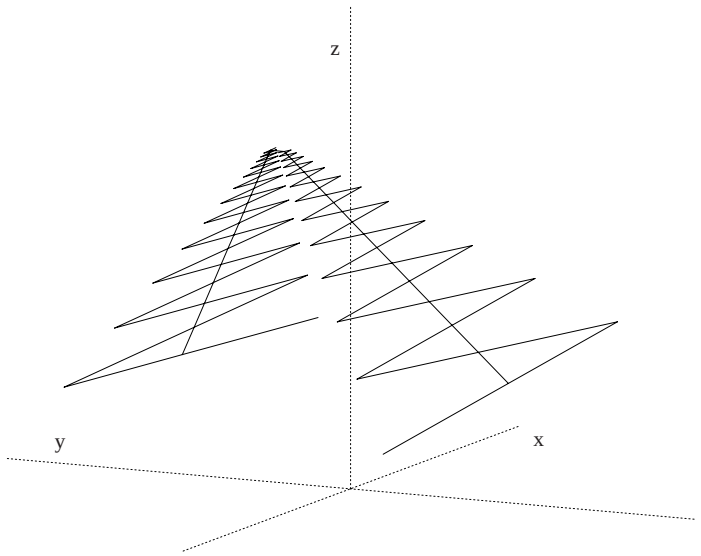

Figure 3.19: Wire model for the optimized log-periodic zigzag antenna as in figure 3.20.

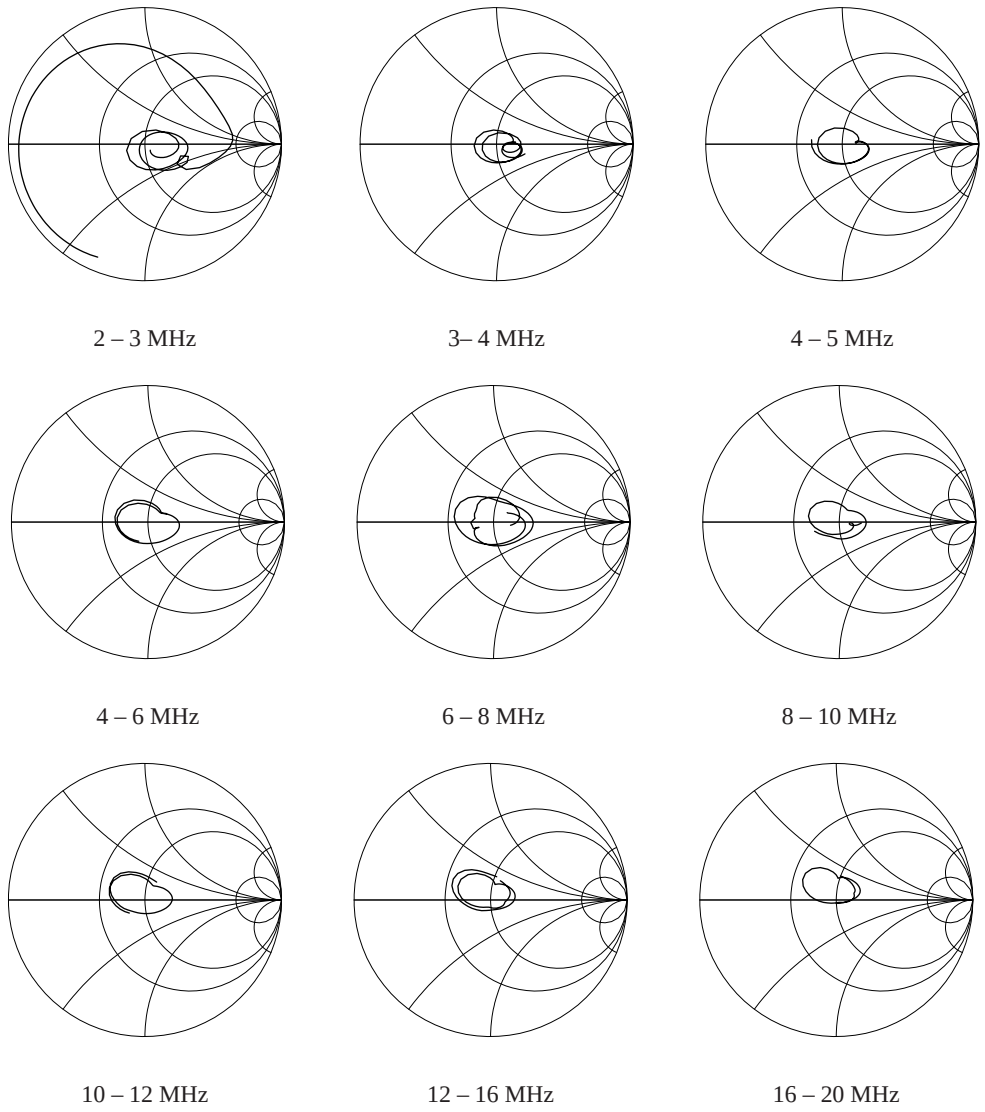

Figure 3.20: Smith-chart representation of the input impedance for the optimized log-periodic zigzag antenna. H = 25.63 m, W = 59.48 m, L = 35.66 m, $w_{\min}$ = 2.5, τ = 0.76, wire diam. = 1.63 mm, $R_{\text{load}} = \infty$, height over ground = 10.65 m, σ = 2 mS/m, ε_{r} = 5, x-position = -4.36 m, y-position = 5.66 m, Z_0 = 300 Ω.

were found to be responsible for the deviation. Namely, as the apex is shifted away from the center, the intersection points between the feed line and the teeth move further away from each other. Consequently, feed and tooth scales are no longer matched. Furthermore, if the apex is shifted along both horizontal axes, the low-frequency antenna performance becomes susceptive for the directions in which the final teeth are pointing.

The preceding design parameters were then optimized to the current antenna location, leading to the final zigzag design displayed in figure 3.19. A Smith chart representation of the input impedance can be found in figure 3.20.

3.6 Evaluation

In connection to the detailed analysis in this chapter, the final design options were compared and evaluated with respect to the specifications stated in the introduction. It was readily apparent that the log-periodic dipole array, because of limitations in height, does not feature the desired broadband impedance pattern. On the other hand, both the pyramidal log-spiral and the log-periodic zigzag antenna feature reasonable input impedance and radiation patterns.

In comparison to the zigzag antenna, the spiral performs better at low frequencies due to its very effective termination and it shows also a lower standing wave ratio over the desired frequency band. However, in order to probe the ionosphere for both polarization modes, two spiral antennas would be necessary. Furthermore, the zigzag antenna is easier to assemble since it contains two, almost independent wire curtains. Therefore, the *log-periodic zigzag* design was finally chosen. All material and construction details are presented in the following chapter.

Chapter 4

Construction

An extension to the existing steel lattice mast on the backyard in order to increase the total antenna-height was considered in an early stage of the project. Detailed antenna simulations indicated that the height of the antenna is vital to its proper broadband performance.

The antenna consists of two curtains with conducting wire, which are spanned between guy ropes supported by a flag pole. The flag pole itself is mounted on a steel lattice mast, and the guy ropes are connected to anchors in the facade of the surrounding building. The final, optimized, antenna design was transfered to a detailed CAD drawing, together with information gathered from original blue prints of the building as well as measurements taken with a laser distance meter. The data holds a measurement uncertainty of approximately one centimeter. A site overview as well as a plane view of the antenna with related parameters can be found in the appendix.

The antenna wire is made up of strands of copper clad steel. The steel core provides mechanical resistance at a very low weight, and the copper coating gives the material good conductivity and resistance to corrosion. Because of the *skin effect*, most of the alternating current flows in the outer part of the wire. The current penetrates the conductor down to the *skin depth*, δ, which is given by

$$\delta = \sqrt{\frac{2\rho}{\omega\mu}},$$

where ρ is the resistivity of the conductor, ω is the angular frequency of the current and μ is the absolute magnetic permeability of the conductor[1]. In conclusion, copper coated wire may perform as well as solid copper wire, as long as the copper coating is thick enough to hold the current at the specific frequency. Properties of the used antenna wire can be found in table 4.1. Aside from the material itself, stranded wire is not as strong as solid wire, but it can withstand repeated bending and twisting much better due to its mechanical flexibility. Furthermore, this flexibility makes it easier to work with during construction.

The antenna rope consists of a combination of different polymer fibers. The core is made of enhanced polyethylene fiber, which has extremely long molecule chains. Because

[1] As an example, the skin depth in copper (μ_{CU} = 1.26 N/A^2; ρ_{CU} = 17 nΩm) at 2.5 MHz is about 30 μm

Table 4.1: Properties of the antenna wire.

Property	Value
Material	19 strands of copper-clad steel (40% copper)
Mass / unit length	17 g/m
Breaking strength	1321 N
Diameter	1.63 mm

Table 4.2: Properties of the guy rope.

Property	Value
Core material	ultra-high molecular weight polyethylene fiber
Cover material	polyester fiber
Mass / unit length	50 g/m
Breaking strength	10 787 N
Diameter	8 mm

of this long chains, the fiber features the highest strength found among polymers, and it stretches very little under tension (2-3%). The rope is sheeted by a braided polyester cover, which provides resistance to ultra-violet radiation and chemicals. All ropes are terminated with thimble fitted loops. Table 4.2 provides a list of properties for the current rope type. Lift as well as anchor ropes are using a standard polyester core.

Intersecting wires are joined through a washer, which preserves the natural shape of the wire. Shearing forces on the material are thereby minimized. Additionally, the connection is secured by soldering and a silicone coat, ensuring good electrical connection as well as long-term flexibility. The antenna wire is connected to the guy ropes with cable ties, a solution that needs very little construction effort.

The antenna is fed through a transmission line, which connects the feed point at the top of the antenna to the amplifier, located inside the Alfvén laboratory. The transmission line is a two-conductor ladder-line with a characteristic impedance of 300 Ohms. The upper end is connected to both antenna curtains through short ropes, with the conducting wires running alongside. Drawings of these details can be found in the appendix.

The flagpole is made of fiber-reinforced polyester, a nonconducting material which is very strong and lightweight. A basic calculation was set up in order to predict the maximum load supported by the structure. However, these calculations approximated the flagpole as a cylinder (with a diameter of $\varnothing_{\text{min}}$) instead of a cone with a varying diameter. Therefore, results were much lower than in reality. In consultation with the mechanics department at the KTH, it was found that a more complex analysis involving a finite element method would be necessary to obtain more accurate results. But such an analysis is quite exhaustive and was thought to be unnecessary for the project at hand. The flagpole is stabilized by four guy ropes which are spanned between the top and four anchor points at the corners of the

Table 4.3: Properties of the flagpole.

Property	Value
Material	Fiber-reinforced polyester
Young's modulus (E_z,E_x)	17 GN/m^2, 8 GN/m^2
Yield strength (σ_3)	250 MN/m^2
Mass	115 kg
Length	18 m
Diameter ($\varnothing_{\min}$,$\varnothing_{\max}$)	65 mm, 175 mm

backyard. These ropes support also the antenna itself. Additionally, four guy ropes are attached at the middle of the flagpole.

The flagpole is also equipped with a conducting wire between its metal top-ring and the mast in order to provide lightning protection. Additionally, high voltages induced into the antenna can be shortened out by a spark gap located close to the antenna feed. This feature, however, was not incorporated in the current design drawings.

The antenna is hoisted via pulleys at the top of the flagpole as well as at the anchor points. Hence, the structure can easily be lowered for maintenance. The pulleys are typical maintenance-free rigging blocks and provide longterm resistance to ultraviolet radiation and severe weather conditions. Because of some elasticity in the ropes as well as in the flagpole, the structure is inherently flexible and should be able to withstand high winds as well as icing.

Wire and rope tension is critical to antenna geometry, but should not exceed the limitations of the flag pole or the anchors. Additionally, other forces like wind or ice will influence the tension needed for proper operation. In consultation with SMHI[2], a maximum wind speed of about 35 m/s and a radial ice thickness of maximal 0.5 mm was assumed for the antenna location. Approximate calculations revealed that the tension on the antenna wires, if optimized to minimal sag, exceeds the maximal tension on the guy ropes for the current configuration.

Another solution to maintain wire tension without exceeding anchor or flagpole limitations is to give the guy ropes a parabolic shape. Consequently, wire tension is transfered to the anchor points more directly. But irregularities in the element length of the log-periodic zigzag antenna have a quite severe impact on input characteristics. As simulations revealed, a change of the zag-length by five procent shifts the input-resistance by the factor of two. Therefore, this solution was not pursued. Additional tension-ropes for the lowermost antenna-wires might become necessary if wire sag becomes too excessive.

[2] **S**veriges **M**eteorologiska och **H**ydrologiska **I**nstitut, Swedish Meteorological and Hydrological Institute

Chapter 5

Conclusion

A transmitter antenna for an ionospheric sounder at the Alfvén Laboratory has been designed. The antenna features a vertical-incidence, linear-polarized radiation pattern for frequencies between 2 and 20Mhz at a standing wave ratio of less than 2:1 and a varying gain between 0 and 6 dBi. The structure spans over the entire backyard of the laboratory with a width of 35 m and a length of 60 m. It is supported by a flagpole mounted on a steel lattice mast giving a total height of about 36 m.

5.1 Summary

Preceding the actual design process, a short antenna type survey revealed that the frequency independent antennas are superior to broadband dipoles and traveling wave antennas in respect to their broadband capabilities. Therefore, the antenna design focused on three frequency independent antennas.

Simulation-models of broadband antennas are usually very large due to the complexity and the bandwidth of broadband antennas. In order to minimize computation time a more flexible, frequency adaptive, segmentation method was developed. The simulation procedure was automated with a script for model generation and verification as well as parameter sweeping and output visualization. While the surrounding buildings only have a minor effect on radiation patterns, the ground plane in close vicinity to the antenna has a profound impact on antenna performance. However, since no distinctive parameters are known, ground reflections were not incorporated into the design, and a so called apex-up design was favored.

Frequency independent antennas radiate only from a finite region of their structure at any given frequency. If this region is not dissipating all available power, other parts of the structure might start to radiate at a given frequency. Thereby, input impedance will shift significantly and antenna performance will deteriorate. This is the case for the log-periodic dipole antenna in this study, since the ratio between adjacent dipole-elements is too excessive. The maximum apex angle for sufficient broadband performance is about 45 degrees.

Unlike the dipole array, both the pyramidal log-spiral as well as the log-periodic zigzag

antenna hold continuous elements. This results in a non-sequential structure which is able to radiate at almost every frequency within the bandwidth of the antenna. Both antenna types were optimized for the current antenna location and provide sufficient broadband performance. Low-frequency performance can be enhanced with resistive loading, which is more successful for the spiral than for the zigzag antenna.

Finally, the log-periodic zigzag antenna was chosen for construction because of its linear polarization and its simple feed arrangement. The antenna consists of stranded antenna wire spanned between guy ropes which are supported from a flagpole down to anchor points at the facade of the surrounding building.

5.2 Discussion

Another type of design procedure using so called genetic algorithms was not used during this study. The amount of optimization and specialization common to antennas of this type was estimated to increase nonlinear behavior. Another implication against these antennas is the absence of accurate ground parameters. However, genetic algorithms might generate an antenna superior to the one designed in this project.

Although fairly complex, the simulation script does not incorporate any optimization procedure. It can be argued that such a feature might have accelerated the overall design process as well as improved the final result. However, due to a fairly complex design process as well as difficult simulation control, no automated optimization was used during simulation.

The special segmentation procedure used in this project disregards certain modelling rules linked to the simulator, but the accuracy of this procedure was verified in numerous simulations. However, further study is implied in order to prove the absolute accuracy for this modelling routine.

Ground parameters were not incorporated into the antenna design since no distinctive values do exist for the current antenna location. Although an apex-down solution might have been superior to the current apex-up design, the later was favored in an early stage of the project due to uncertain ground parameters, as well as the reduced construction effort of this design. Additionally, the actual antenna location has presumably poor conductivity and is therefore not suited for apex-down designs.

Resistive loading of the structure is proposed and simulated, but not included into the final design. This improvement is considered for future work on the real antenna.

A detailed analysis of the mechanical forces inside the antenna structure has been omitted due to its complexity. Nonetheless, such an analysis would provide a more accurate safety-estimate of the structural strength in general and of the flagpole in particular. Furthermore, wire and rope tension could have been optimized for optimal wire sag and structural stress limits. However, a detailed analysis of the mechanical forces exceeds the scope of this thesis.

Bibliography

Balanis, C. *Antenna theory. Analysis and design.* John Wiley & Sons, 3rd edition [2005]. ISBN 0-471-66782-X.

Bell, R., Elfving, C., and Franks, R. Near-field measurements on a logarithmically periodic antenna. *Antennas and Propagation, IEEE Transactions on [legacy, pre - 1988]*, 8(6):559–567 [1960]. ISSN 0096-1973.

Bruce, E., Beck, A., and Lowry, L. Horizontal rhombic antennas. *Proceedings of the IRE*, 23(1):24–46 [1935]. ISSN 0096-8390.

Cathey, J., W. and Beck, F. Radiation patterns of the logarithmic spiral antenna on an elliptical cone. *Antennas and Propagation, IEEE Transactions on [legacy, pre - 1988]*, 12(4):491–492 [1964]. ISSN 0096-1973.

Cebik, L. B. Notes on the terminated wide-band ”folded dipole” [2000]. URL `http://www.cebik.com/wire/wbfd.html`. Retrieved on 2007-09-27.

Cebik, L. B., Hallidy, D., Jansson, D., and Lewallen, R. *ARRL Antenna Book*. American Radio Relay League, 21st edition [2007]. ISBN 0872599876.

Coro, A. How to build the ttfd-2: A broadband antenna for shortwave recepetion and transmission [2007]. URL `http://www.radiohc.cu/ingles/dxers/dxers2007/antena.htm`. Retrieved on 2007-09-27.

Dheim, M. N. A. *Broadband Active Antenna*. Master’s thesis, Royal Institute of Technology (KTH) [2008].

Dietrich, F. and Long, R. An efficient moderate-size vertical-incidence ionosonde antenna for 2-20-mhz polarization studies. *Antennas and Propagation, IEEE Transactions on [legacy, pre - 1988]*, 17(5):551–557 [1969]. ISSN 0096-1973.

DuHamel, R. and Isbell, D. Broadband logarithmically periodic antenna structures. In D. Isbell, editor, *IRE International Convention Record*, volume 5, pages 119–128 [1957].

DuHamel, R. and Ore, F. Logarithmically periodic antenna designs. In F. Ore, editor, *IRE International Convention Record*, volume 6, pages 139–151 [1958].

Dyson, J. The equiangular spiral antenna. *Antennas and Propagation, IEEE Transactions on [legacy, pre - 1988]*, 7(2):181–187 [1959a]. ISSN 0096-1973.

Dyson, J. The unidirectional equiangular spiral antenna. *Antennas and Propagation, IEEE Transactions on [legacy, pre - 1988]*, 7(4):329–334 [1959b]. ISSN 0096-1973.

Dyson, J. The characteristics and design of the conical log-spiral antenna. *Antennas and Propagation, IEEE Transactions on [legacy, pre - 1988]*, 13(4):488–499 [1965]. ISSN 0096-1973.

Greiser, J. and Mayes, P. The bent backfire zigzag – a vertically-polarized frequency-independent antenna. *Antennas and Propagation, IEEE Transactions on [legacy, pre - 1988]*, 12(3):281–290 [1964]. ISSN 0096-1973.

Hertel, T. and Smith, G. Analysis and design of two-arm conical spiral antennas. *Electromagnetic Compatibility, IEEE Transactions on*, 44(1):25–37 [2002]. ISSN 0018-9375.

Isbell, D. Log periodic dipole arrays. *Antennas and Propagation, IEEE Transactions on [legacy, pre - 1988]*, 8(3):260–267 [1960]. ISSN 0096-1973.

Kraus, J. D. and Marhefka, R. J. *Antennas. For All Applications*. McGraw-Hill series in electrical engineering. McGraw-Hill, 3rd edition [2002]. ISBN 0-07-232103-2.

Lee, S. and Mei, K. Analysis of zigzag antennas. *Antennas and Propagation, IEEE Transactions on [legacy, pre - 1988]*, 18(6):760–764 [1970]. ISSN 0096-1973.

Mayes, P. Frequency-independent antennas and broad-band derivatives thereof. *Proceedings of the IEEE*, 80(1):103–112 [1992]. ISSN 0018-9219.

Richeson, P. D. Nec-2 manual, part iii: User's guide [1996]. URL `http://www.nec2.org/other/nec2prt3.pdf`. Retrieved on 2007-10-08.

Rumsey, V. Frequency independent antennas. In *IRE International Convention Record*, volume 5, pages 114–118 [1957].

Sivan-Sussman, R. Various modes of the equiangular spiral antenna. *Antennas and Propagation, IEEE Transactions on [legacy, pre - 1988]*, 11(5):533–539 [1963]. ISSN 0096-1973.

Tang, C. A class of modified log-spiral antennas. *Antennas and Propagation, IEEE Transactions on [legacy, pre - 1988]*, 11(4):422–427 [1963]. ISSN 0096-1973.

Thewlis, J., Glass, R., Hughes, D., and Meetham, A. *Encyclopaedic dictionary of physics*, volume Vols. 1-9, A to Z. Pergamon Press [1961].

Tsukiji, T. and Tou, S. Impedance characteristics of polygonal loop antennas. In S. Tou, editor, *Antennas and Propagation Society International Symposium, 1979*, volume 17, pages 396–399 [1979].

Tsukiji, T. and Tou, S. On polygonal loop antennas. *Antennas and Propagation, IEEE Transactions on [legacy, pre - 1988]*, 28(4):571–575 [1980]. ISSN 0096-1973.

Whitten, R. C. and Poppoff, I. G. *Physics of the lower ionosphere*. Prentice-Hall [1965].

Xiaorong, Y., Xiaoguo, L., and Guangyou, F. Computer-aided design of four wire dual-mode spiral antenna. In L. Xiaoguo, editor, *Antennas, Propagation and EM Theory, 2000. Proceedings. ISAPE 2000. 5th International Symposium on*, pages 26–28 [2000].

Yang, L.-B. and Iizuka, K. Experimental investigation on a method of lowering the silhouette of conical log-spiral antenna. *Antennas and Propagation, IEEE Transactions on [legacy, pre - 1988]*, 31(2):347–352 [1983]. ISSN 0096-1973.

Yeh, Y. and Mei, K. Theory of conical equiangular-spiral antennas: Part i–numerical technique. *Antennas and Propagation, IEEE Transactions on [legacy, pre - 1988]*, 15(5):634–639 [1967]. ISSN 0096-1973.

Appendix

KTH Electrical Engineering
100 44 STOCKHOLM
www.ee.kth.se

ALFVÉN LAB. IONOSONDE

TRANSMITTER ANTENNA

SITE OVERVIEW

PAGE	SCALE	DATE	AUTHOR
1/3	1:500	2008-05-29	ALEXANDER WITTE

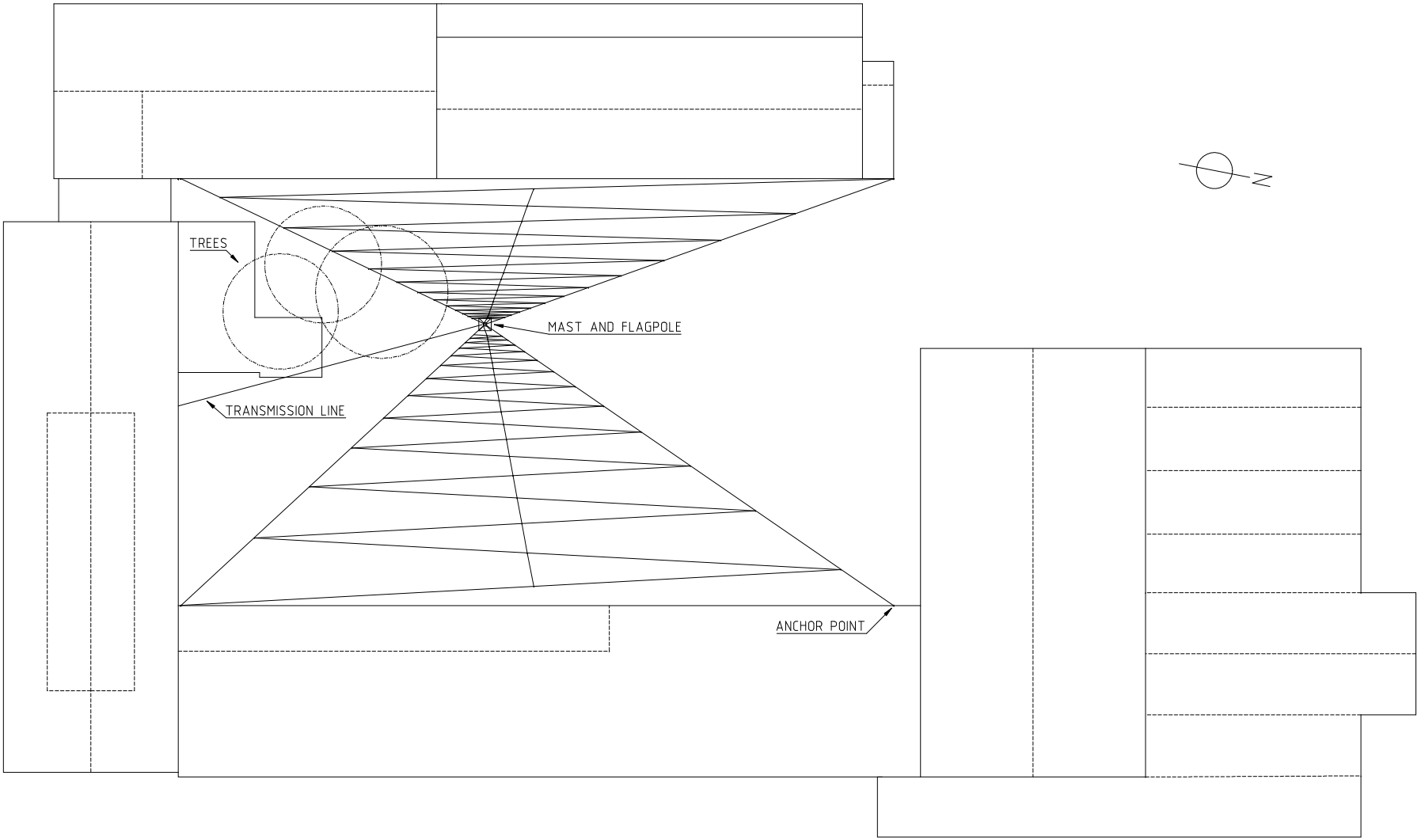

KTH Electrical Engineering
100 44 STOCKHOLM
www.ee.kth.se

ALFVÉN LAB. IONOSONDE

TRANSMITTER ANTENNA

PLANE VIEW

PAGE	SCALE	DATE	AUTHOR
2/3	1:500	2008-05-29	ALEXANDER WITTE

ALL LENGTHS IN METER

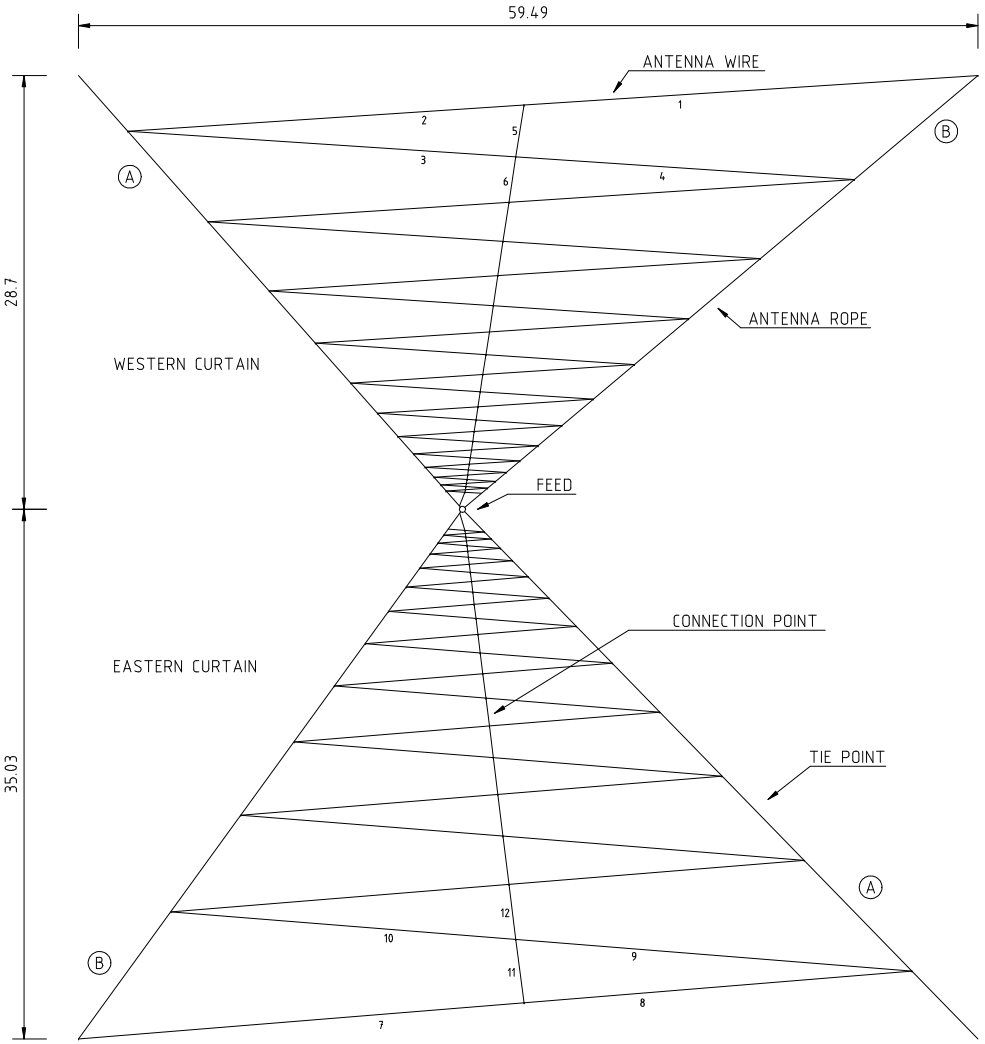

PARAMETERS

GEOMETRIC RATIO τ = 0.76
ANCHOR HEIGHT = 10.652
TOTAL HEIGHT = 36.65
WIDTH = 59.48
LENGTH = 35.66
APEX DEVIATION = 4.36, 5.66

TIE POINTS

DELTA / DISTANCE TO APEX

ROPE A		*ROPE B*	
EASTERN CURTAIN			
0.50	2.08	0.51	2.11
0.66	2.74	0.67	2.78
0.87	3.61	0.88	3.66
1.14	4.74	1.16	4.82
1.50	6.24	1.52	6.34
1.97	8.21	2.00	8.34
2.59	10.81	2.63	10.97
3.41	14.22	3.46	14.43
4.49	18.71	4.56	18.99
5.91	24.62	6.00	24.99
7.77	32.39	7.89	32.88
10.23	42.62	10.38	43.26
WESTERN CURTAIN			
0.39	1.63	0.52	2.18
0.52	2.15	0.69	2.87
0.68	2.83	0.90	3.77
0.89	3.72	1.19	4.96
1.17	4.89	1.57	6.53
1.54	6.44	2.06	8.59
2.03	8.47	2.71	11.30
2.67	11.14	3.57	14.87
3.52	14.66	4.70	19.57
4.63	19.29	6.18	25.75
6.09	25.39	8.13	33.88
8.02	33.40	10.70	44.57

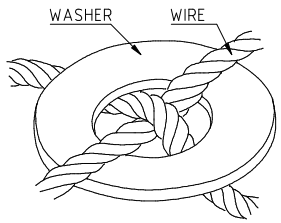

CONNECTION POINT DETAIL

WIRES

NO. / LENGTH

WESTERN CURTAIN		EASTERN CURTAIN	
1	30.103	7	29.539
2	26.243	8	25.752
3	25.724	9	26.271
4	22.425	10	22.902
5	3.468	11	4.217
6	3.023	12	3.676
13	22.878	19	22.450
14	19.945	20	19.571
15	19.550	21	19.966
16	17.043	22	17.406
17	2.636	23	3.205
18	2.298	24	2.794
25	17.387	31	17.062
26	15.158	32	14.874
27	14.858	33	15.174
28	12.953	34	13.228
29	2.003	35	2.436
30	1.746	36	2.123
37	13.214	43	12.967
38	11.520	44	11.304
39	11.292	45	11.532
40	9.844	46	10.053
41	1.522	47	1.851
42	1.327	48	1.614
49	10.043	55	9.855
50	8.755	56	8.591
51	8.582	57	8.764
52	7.482	58	7.641
53	1.157	59	1.407
54	1.009	60	1.227
61	7.633	67	7.490
62	6.654	68	6.529
63	6.522	69	6.661
64	5.686	70	5.807
65	0.879	71	1.069
66	0.767	72	0.932
73	5.801	79	5.692
74	5.057	80	4.962
75	4.957	81	5.062
76	4.321	82	4.413
77	0.668	83	0.813
78	0.583	84	0.708
85	4.409	91	4.326
86	3.843	92	3.771
87	3.767	93	3.847
88	3.284	94	3.354
89	0.508	95	0.618
90	0.443	96	0.538
97	3.351	103	3.288
98	2.921	104	2.866
99	2.863	105	2.924
100	2.496	106	2.549
101	0.386	107	0.469
102	0.336	108	0.409
109	2.546	115	2.499
110	2.220	116	2.178
111	2.176	117	2.222
112	1.897	118	1.937
113	0.293	119	0.357
114	0.256	120	0.311
121	1.935	127	1.899
122	1.687	128	1.656
123	1.654	129	1.689
124	1.442	130	1.472
125	0.223	131	0.271
126	0.194	132	0.236
133	1.471	138	1.443
134	1.282	139	1.258
135	1.257	140	1.284
136	1.096	141	1.119
137	0.169	142	0.206

KTH Electrical Engineering
100 44 STOCKHOLM
www.ee.kth.se

ALFVÉN LAB. IONOSONDE

TRANSMITTER ANTENNA

FEED AND RIGGING

PAGE	SCALE	DATE	AUTHOR
3/3	1:5	2008-05-29	ALEXANDER WITTE

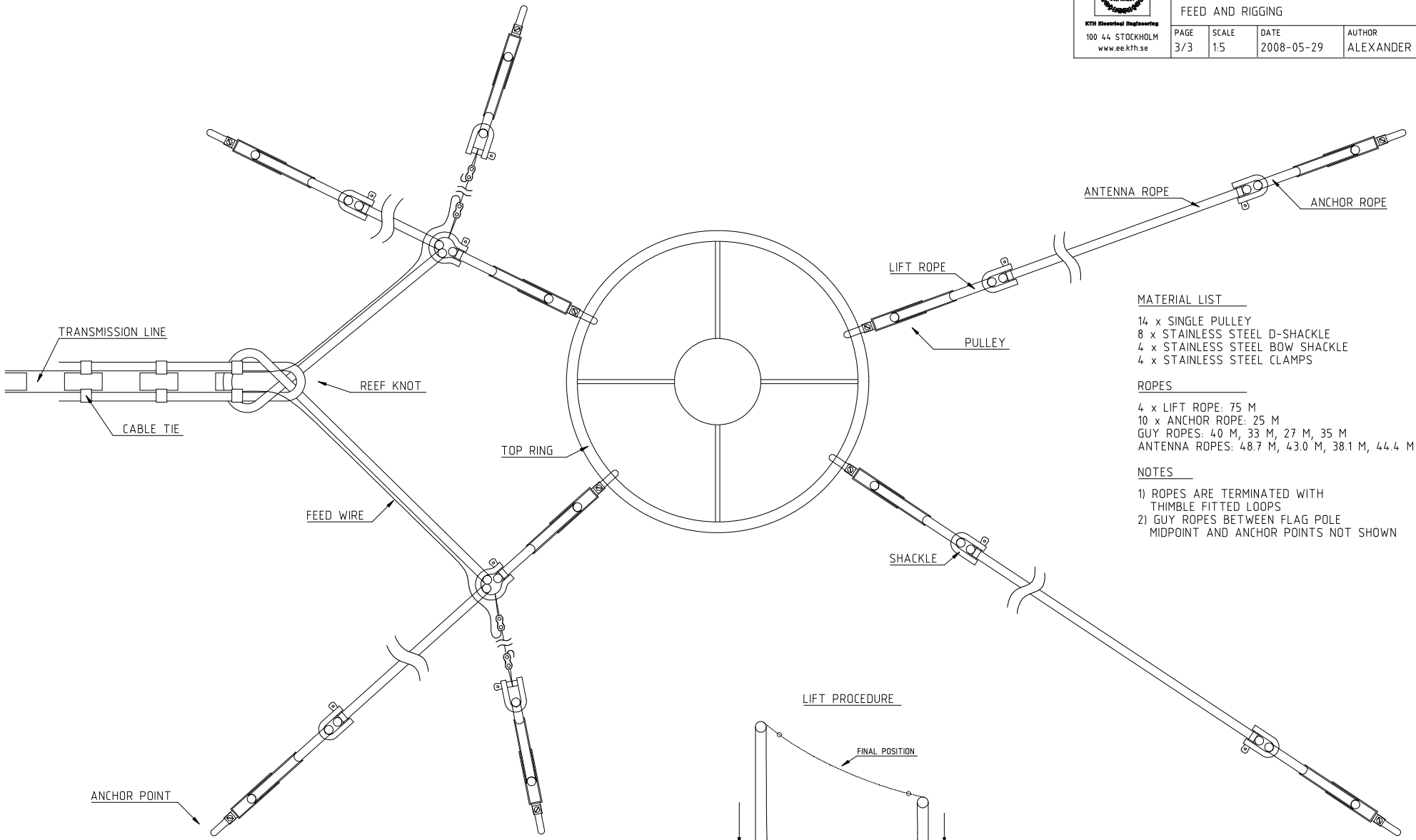

MATERIAL LIST

14 x SINGLE PULLEY
8 x STAINLESS STEEL D-SHACKLE
4 x STAINLESS STEEL BOW SHACKLE
4 x STAINLESS STEEL CLAMPS

ROPES

4 x LIFT ROPE: 75 M
10 x ANCHOR ROPE: 25 M
GUY ROPES: 40 M, 33 M, 27 M, 35 M
ANTENNA ROPES: 48.7 M, 43.0 M, 38.1 M, 44.4 M

NOTES

1) ROPES ARE TERMINATED WITH THIMBLE FITTED LOOPS
2) GUY ROPES BETWEEN FLAG POLE MIDPOINT AND ANCHOR POINTS NOT SHOWN

LIFT PROCEDURE